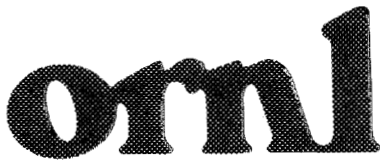




3 4456 0420027 3

ORNL/TM-12813 (Part 3)



**OAK RIDGE  
NATIONAL  
LABORATORY**



**New Insights into Input Relegation  
Control for Inverse Kinematics of a  
Redundant Manipulator  
Part 3: An Application to Joint Limit  
Avoidance**

M. A. Unseren

OAK RIDGE NATIONAL LABORATORY  
 CENTRAL RESEARCH LIBRARY  
 CIRCULATION SECTION  
 4007H ROOM 175  
**LIBRARY LOAN COPY**  
 DO NOT TRANSFER TO ANOTHER PERSON  
 If you wish someone else to see this  
 report, send in name with report and  
 the library will arrange a loan.  
 #ORNL-12813-375

MANAGED BY  
MARTIN MARIETTA ENERGY SYSTEMS, INC.  
FOR THE UNITED STATES  
DEPARTMENT OF ENERGY

This report has been reproduced directly from the best available copy.

Available to DOE and DOE contractors from the Office of Scientific and Technical Information, P.O. Box 62, Oak Ridge, TN 37831; prices available from (615) 576-8401, FTS 626-8401.

Available to the public from the National Technical Information Service, U.S. Department of Commerce, 5285 Port Royal Rd., Springfield, VA 22161.

NTIS price codes—Printed Copy: A03 Microfiche A01

This report was prepared as an account of work sponsored by an agency of the United States Government. Neither the United States Government nor any agency thereof, nor any of their employees, makes any warranty, express or implied, or assumes any legal liability or responsibility for the accuracy, completeness, or usefulness of any information, apparatus, product, or process disclosed, or represents that its use would not infringe privately owned rights. Reference herein to any specific commercial product, process, or service by trade name, trademark, manufacturer, or otherwise, does not necessarily constitute or imply its endorsement, recommendation, or favoring by the United States Government or any agency thereof. The views and opinions of authors expressed herein do not necessarily state or reflect those of the United States Government or any agency thereof.

295

Computer Science and Mathematics Division

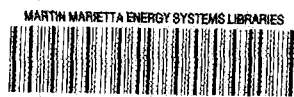
**NEW INSIGHTS INTO INPUT RELEGATION CONTROL FOR INVERSE  
KINEMATICS OF A REDUNDANT MANIPULATOR  
PART 3: AN APPLICATION TO JOINT LIMIT AVOIDANCE**

M. A. Unseren

Center for Engineering Systems Advanced Research

DATE PUBLISHED: JULY, 1995

Prepared by  
Oak Ridge National Laboratory  
Oak Ridge, Tennessee 37831  
managed by  
LOCKHEED MARTIN ENERGY SYSTEMS, INC.  
for the  
U. S. DEPARTMENT OF ENERGY  
under Contract No. DE-AC05-84OR21400



3 4456 0420027 3



# CONTENTS

List of Figures.....	v
List of Tables.....	ix
Abstract.....	xi
1. Introduction.....	1
2. Problem Statement.....	3
3. Calculation of Corrective Action.....	5
3.1 Linear Function Method.....	5
3.2 Cycloidal Function Method.....	7
4. Numerial Simulation Studies.....	13
5. Conclusion.....	67
6. Acknowledgement.....	69
References.....	71



## LIST OF FIGURES

<u>Figure</u>	<u>Page</u>
1. Trajectory of $\dot{q}_1^*$ (Linear Method) .....	6
2. Trajectory of $d\dot{q}_1^*/dq_1$ (Linear Method) .....	6
3. Trajectory of $\dot{q}_1^*$ (Cycloidal Method) .....	10
4. Trajectory of $d\dot{q}_1^*/dq_1$ (Cycloidal Method) .....	10
5. Trajectory of $\ddot{q}_1^*$ (Cycloidal Method) .....	11
6. Trajectory of $d\ddot{q}_1^*/dq_1$ (Cycloidal Method) .....	11
1.F1 Fan Plot With No JLA (Case 1) .....	17
1.F2 Fan Plot Using Linear JLA Method .....	17
1.F3 Fan Plot Using Cycloidal JLA Method .....	17
1.J1A Trajectories for Joint One (Entire Range of Motion) .....	18
1.J1B Trajectories for Joint One (Range Where JLA is Active) .....	19
1.J2A Trajectories for Joint Two (Entire Range of Motion) .....	20
1.J2B Trajectories for Joint Two (Range Where JLA is Active) .....	21
1.J3A Trajectories for Joint Three (Entire Range of Motion) .....	22
1.J3B Trajectories for Joint Three (Range Where JLA is Active) .....	23
1.J4A Trajectories for Joint Four (Entire Range of Motion) .....	24
1.J4B Trajectories for Joint Four (Range Where JLA is Active) .....	25
2.F1 Fan Plot With No JA (Case 2) .....	27
2.F2 Fan Plot Using Linear JLA Method .....	27
2.F3 Fan Plot Using Cycloidal JLA Method .....	27
2.J1A Trajectories for Joint One (Entire Range of Motion) .....	28

2J1B Trajectories for Joint One (Range Where JLA is Active) .....	29
2J2A Trajectories for Joint Two (Entire Range of Motion) .....	30
2J2B Trajectories for Joint Two (Range Where JLA is Active) .....	31
2J3A Trajectories for Joint Three (Entire Range of Motion) .....	32
2J3B Trajectories for Joint Three (Range Where JLA is Active) .....	33
2J4A Trajectories for Joint Four (Entire Range of Motion) .....	34
2J4B Trajectories for Joint Four (Range Where JLA is Active) .....	35
3.F1 Fan Plot With No JLA (Case 3) .....	37
3.F2 Fan Plot Using Linear JLA Method .....	37
3.F3 Fan Plot Using Cycloidal JLA Method .....	37
3J1A Trajectories for Joint One (Entire Range of Motion) .....	38
3J1B Trajectories for Joint One (Range Where JLA is Active) .....	39
3J2A Trajectories for Joint Two (Entire Range of Motion) .....	40
3J2B Trajectories for Joint Two (Range Where JLA is Active) .....	41
3J3A Trajectories for Joint Three (Entire Range of Motion) .....	42
3J3B Trajectories for Joint Three (Range Where JLA is Active) .....	43
3J4A Trajectories for Joint Four (Entire Range of Motion) .....	44
3J4B Trajectories for Joint Four (Range Where JLA is Active) .....	45
4.F1 Fan Plot With No JLA (Case 4) .....	47
4.F2 Fan Plot Using Linear JLA Method .....	47
4.F3 Fan Plot Using Cycloidal JLA Method .....	47
4J1A Trajectories for Joint One (Entire Range of Motion) .....	48
4J1B Trajectories for Joint One (Range Where JLA is Active) .....	49
4J2A Trajectories for Joint Two (Entire Range of Motion) .....	50
4J2B Trajectories for Joint Two (Range Where JLA is Active) .....	51

4.J3A Trajectories for Joint Three (Entire Range of Motion) .....	52
4.J3B Trajectories for Joint Three (Range Where JLA is Active) .....	53
4.J4A Trajectories for Joint Four (Entire Range of Motion) .....	54
4.J4B Trajectories for Joint Four (Range Where JLA is Active) .....	55
5.F1 Fan Plot With No JLA (Case 5) .....	57
5.F2 Fan Plot Using Linear JLA Method .....	57
5.F3 Fan Plot Using Cycloidal JLA Method .....	57
5.J1A Trajectories for Joint One (Entire Range of Motion) .....	58
5.J1B Trajectories for Joint One (Range Where JLA is Active) .....	59
5.J2A Trajectories for Joint Two (Entire Range of Motion) .....	60
5.J2B Trajectories for Joint Two (Range Where JLA is Active) .....	61
5.J3A Trajectories for Joint Three (Entire Range of Motion) .....	62
5.J3B Trajectories for Joint Three (Range Where JLA) .....	63
5.J4A Trajectories for Joint Four (Entire Range of Motion) .....	64
5.J4B Trajectories for Joint Four (Range Where JLA is Active) .....	65



## LIST OF TABLES

<u>Table</u>	<u>Page</u>
1. Link Lengths .....	13
2. Case One Parameters .....	13
3. Case Two Parameters .....	14
4. Case Three Parameters .....	14
5. Case Four Parameters .....	15
6. Case Five Parameters .....	15



### Abstract

In Part 2 of this report [6], it was argued that a single secondary performance criteria defined as the square of the Euclidean norm of the error between the vector of joint velocities  $\dot{q}$  and a vector of "corrective" joint velocities  $\dot{q}^*$  can be minimized using input relegation control to yield a solution for  $\dot{q}$  that satisfies the end effector trajectory tracking requirement for an  $N$  joint, serial link redundant manipulator. The solution is an explicit function of  $\dot{q}^*$ . In Part 3 of this report, a new approach for joint limit avoidance during motion of the manipulator is presented which requires defining ranges of motion in close proximity to the upper and lower physical hardware limits of each joint by specifying upper and lower tolerances, respectively. When a joint lies in either of these ranges, it is regarded that a shutdown or damage to the manipulator are imminent due to the joint reaching a limit. Therefore when one or more joints lie within their respective prohibitive outer ranges, two methods for calculating the corrective joint velocities  $\dot{q}_i^*$  corresponding to those joints are proposed. In both methods a corrective velocity is calculated as a scaled function of the maximum allowable velocity for the joint whose magnitude is based on how close the joint is to its limit. On the other hand, when a joint does not lie in either prohibitive outer range, the corrective velocity corresponding to that joint is set to zero. The effectiveness of the proposed joint limit avoidance scheme is demonstrated by simulation studies. The approach is compared to how others have solved the joint limit avoidance problem using the gradient projection scheme [3, 4, 5].



# 1 Introduction

When an open chain, serial link kinematically redundant manipulator performs on-line end-effector trajectory tracking, the joint space trajectories cannot be predicted in advance [1]. Indeed, the inverse kinematics problem for such a manipulator is underspecified, and there exists infinitely many joint configurations for a given end-effector configuration [2]. Thus, unless a joint limit avoidance criteria is incorporated into the inverse kinematics, there exists a possibility that one or more joints may reach their physical hardware limits.

The primary approach to avoiding joint limits has been accomplished using the gradient projection technique. It was originally proposed in [3] and thoroughly investigated in [4, 5]. In these works a scalar function  $g(q)$  representing a secondary performance criteria to be optimized was introduced:

$$g = (q - q^{dp})^T (q - q^{dp}) \quad (1)$$

where  $q^{dp}$  is an  $(N \times 1)$  vector of desired joint positions, e.g.,  $q_i^{dp}$  might be selected as the midpoint of the entire range of motion for joint  $i$  [5]:

$$q_i^{dp} = \frac{q_i^{max} + q_i^{min}}{2} \quad (2)$$

where  $q_i^{max}$  and  $q_i^{min}$  denote the absolute, physical maximum and minimum hardware limits in the range of joint  $i$  ( $i = 1, 2, \dots, N$ ), respectively.

The proposed solution for the joint velocities obtained by [3, 4, 5] is given in eq. (1)<sup>†1</sup> where the gradient of  $g$  is defined by:

$$\left(\frac{dg}{dq}\right)^T = 2(q - q^{dp}) \quad (3)$$

It is highly improbable that the manipulator joint configuration  $q = q^{dp}$  will ever be achieved while satisfying the end effector trajectory tracking requirement. Thus the second term to the right of eq. (1)<sup>†</sup> will always have to be computed using the joint limit avoidance scheme suggested in [3, 4, 5]. But there exists a multitude of manipulator configurations where all joint angles are sufficiently away from the physical hardware limits. In these cases why should one continue to optimize the joint limit criteria so as to induce each joint to move to a single point  $q_i^{dp}$  in its range? This is very unclear and constitutes a waste of computational effort.

In this report, a contrary view is taken; namely, that a joint limit avoidance scheme should be activated only when it is detected, by sensing, that one or more joints of the manipulator are in close proximity of their upper or lower physical hardware limits. In our approach, ranges of motion in close proximity to the upper and lower physical hardware limits of each joint are defined by specifying upper and lower tolerances, respectively. When one or more joints lie within these prohibitive ranges of motion, two methods for calculating the corrective velocity vector  $\dot{q}^*$  introduced in eq. (3)<sup>†</sup> are presented which tend to move these joints out of the prohibitive ranges by self motion of the manipulator when used in conjunction with the performance criteria and optimization procedure discussed in Part 2.

---

<sup>1</sup>Superscript † denotes that the referenced equation is in Part 2 of this report [6]



## 2 Problem Statement

This report proposes a scheme for incorporating a joint limit avoidance capability during motion of a kinematically redundant manipulator. Introduce the positive, constant angles  $tol_i^{hi}$  and  $tol_i^{lo}$  to define the ranges  $(q_i^{max} - tol_i^{hi}) \leq q_i \leq q_i^{max}$  and  $q_i^{min} \leq q_i \leq (q_i^{min} + tol_i^{lo})$ ,  $i = 1, 2, \dots, N$ . When  $q_i$  lies within either of these ranges, it is regarded that a shutdown and damage to the manipulator are imminent due to the joint reaching a limit. Accordingly, a corrective action is desired to drive joint  $i$  back into the range  $(q_i^{min} + tol_i^{lo}) < q_i < (q_i^{max} - tol_i^{hi})$ . Such corrective action is to be accomplished by inducing a self motion in the manipulator joints, which does not affect end-effector trajectory tracking.

The problem is to calculate a "corrective" velocity for joint  $i$  signified by  $\dot{q}_i^*$  which tends to drive the joint back towards the range  $(q_i^{min} + tol_i^{lo}) < q_i < (q_i^{max} - tol_i^{hi})$  whenever it lies in either of the aforementioned prohibitive ranges.  $\dot{q}_i^*$  is the  $i$ th component of the "corrective" velocity vector  $\dot{q}^*$  introduced in eq. (3)<sup>†</sup>.



### 3 Calculation of Corrective Action

The specific corrective action proposed is to calculate a joint velocity  $\dot{q}_i^*$  whose method of computation is dependent on which range joint  $i$  is lying in.  $\dot{q}_i^*$  is a function of the state of the redundant system, which is known through feedback of the joint variables. Two methods for its calculation are suggested.

#### 3.1 Linear Function Method

$\dot{q}_i^*$  is calculated for each and every joint  $i$  ( $= 1, 2, \dots, N$ ) based on the following conditional algorithm:

$$q_i^{min} \leq q_i \leq (q_i^{min} + tol_i^{lo}) :$$

$$\dot{q}_i^* = \frac{z_i \dot{q}_i^{max}}{tol_i^{lo}} (q_i^{min} + tol_i^{lo} - q_i) \quad (4)$$

$$(q_i^{min} + tol_i^{lo}) < q_i < (q_i^{max} - tol_i^{hi}) :$$

$$\dot{q}_i^* = 0 \quad (5)$$

$$(q_i^{max} - tol_i^{hi}) \leq q_i \leq q_i^{max} :$$

$$\dot{q}_i^* = \frac{z_i \dot{q}_i^{max}}{tol_i^{hi}} (q_i^{max} - tol_i^{hi} - q_i) \quad (6)$$

where  $\dot{q}_i^{max}$  ( $> 0$ ) denotes the peak or maximum time rate of change of joint  $i$  and where it is implicitly assumed that  $tol_i^{hi} > 0$  and  $tol_i^{lo} > 0$ . The quantities  $q_i^{max}$  and  $q_i^{min}$  are defined in conjunction with eq. (2). Please note that the values of the constant quantities  $\{q_i^{max}, q_i^{min}, \dot{q}_i^{max}\}$  are obtained based on the physical limitations of a particular manipulator as noted in its design specifications. In eqs. (4) and (6),  $z_i$  is a constant scaling factor whose value is restricted to the range:

$$0 < z_i \leq 1. \quad (7)$$

$z_i$  is introduced to enable the designer to specify a scaled peak joint velocity ( $z_i \dot{q}_i^{max}$ ) for joint  $i$  in the limit avoidance scheme.

Eq. (6) is the equation of a straight line connecting the points  $(q_i = q_i^{max} - tol_i^{hi}, \dot{q}_i^* = 0)$  and  $(q_i = q_i^{max}, \dot{q}_i^* = -z_i \dot{q}_i^{max})$ . Likewise, eq. (4) is the equation of a straight line connecting the points  $(q_i^{min} + tol_i^{lo}, 0)$  and  $(q_i^{min}, z_i \dot{q}_i^{max})$ . It is easy to see that  $\dot{q}_i^*$  is negative when calculated by eq. (6). This is logical since it is desired to move joint  $i$  away from the upper hardware limit. By the same reasoning  $\dot{q}_i^*$  is positive when evaluated using eq. (4).

*Example 1.* The range of motion for joint no. 1 of the CESARm research manipulator [7, 8, 9] is  $-135^\circ \leq q_1 \leq 44^\circ$ . Its maximum rated velocity is  $\dot{q}_1^{max} = 57.296$  (deg/sec). Suppose we select  $z_1 = 1.0$  and  $tol_1^{hi} = tol_1^{lo} = 15^\circ$ . The trajectory of  $\dot{q}_1^*$  versus  $q_1$  is shown in Figure 1, where eqs. (4) - (6) have been applied.

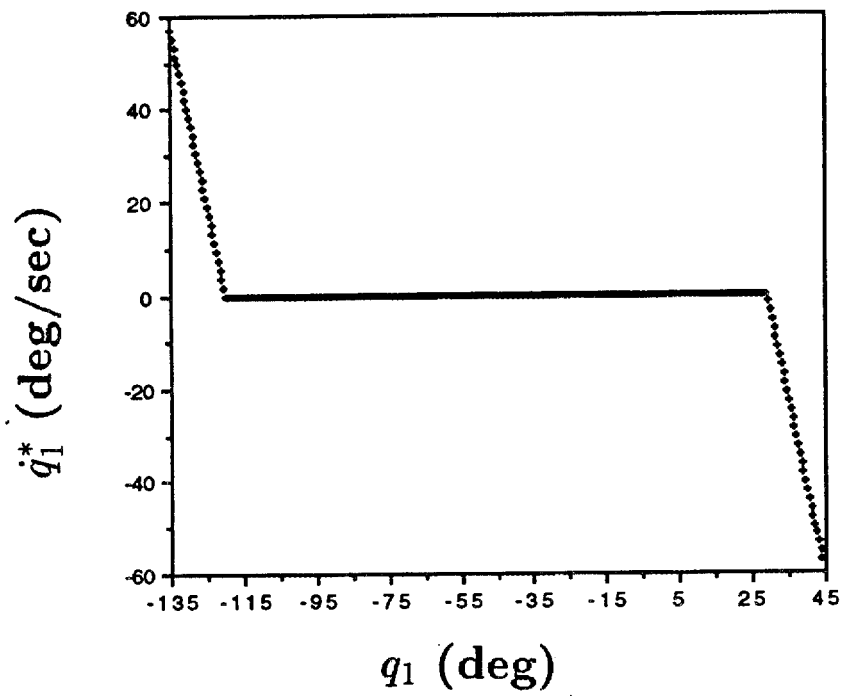


Figure 1. Trajectory of  $\dot{q}_1^*$  (Linear Method)

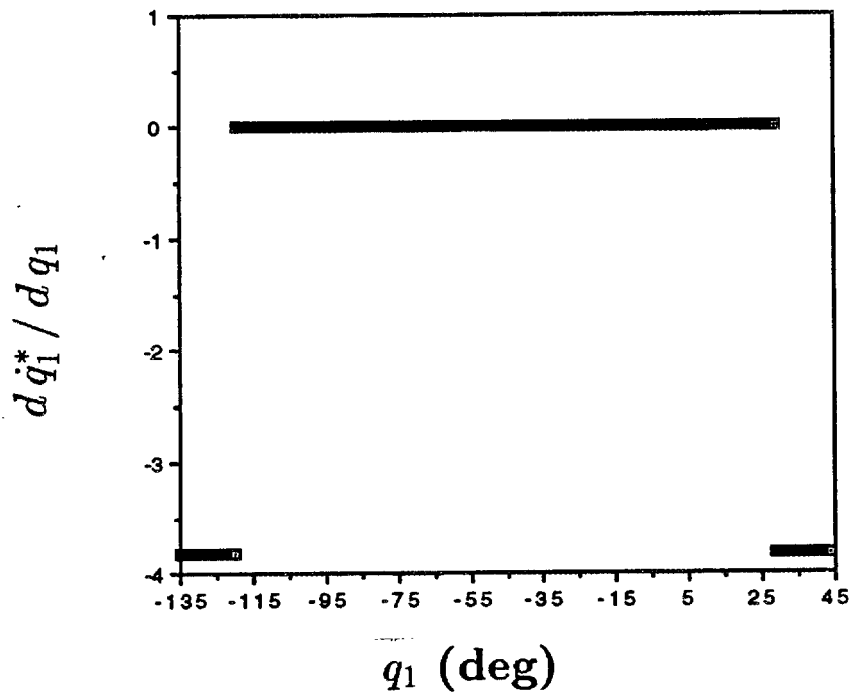


Figure 2. Trajectory of  $d\dot{q}_1^*/dq_1$  (Linear Method)

The term in eq. (10)<sup>†</sup> that is explicit in  $\dot{q}^*$  vanishes whenever all of the joints lie within their respective center (innermost) ranges. For example, in a software program controlling a redundant manipulator using the joint limit avoidance algorithm, a flag would be set only when at least one of the components of  $\dot{q}^*$  is non-zero. Only when that flag is set would the second term to the right of eq. (10)<sup>†</sup> be calculated. This idea could be extended to compute only those columns of the coefficient matrix of  $\dot{q}^*$  in eq. (10)<sup>†</sup> which correspond to those components  $\dot{q}_i^*$  which are nonzero. This approach reduces the computational burden and in the case where  $\dot{q}^* = 0_{N \times 1}$ , yields a minimum Euclidean norm solution for the joint velocities. It supports our contention that the redundant DOF and the Cartesian DOF should not be treated with equal priorities.

The function  $\dot{q}_i^*$  as defined by eqs. (4) - (6) is both sectionally smooth and uniformly continuous. However, the derivative of  $\dot{q}_i^*$  with respect to  $q_i$  as defined by:

$$q_i^{\min} \leq q_i \leq (q_i^{\min} + tol_i^{lo}) : \quad \frac{d \dot{q}_i^*}{d q_i} = - \frac{z_i \dot{q}_i^{\max}}{tol_i^{lo}} \quad (8)$$

$$(q_i^{\min} + tol_i^{lo}) < q_i < (q_i^{\max} - tol_i^{hi}) : \quad \frac{d \dot{q}_i^*}{d q_i} = 0 \quad (9)$$

$$(q_i^{\max} - tol_i^{hi}) \leq q_i \leq q_i^{\max} : \quad \frac{d \dot{q}_i^*}{d q_i} = - \frac{z_i \dot{q}_i^{\max}}{tol_i^{hi}} \quad (10)$$

reveals that function  $\dot{q}_i^*$  is not pointwise differentiable at  $q_i = q_i^{\min} + tol_i^{lo}$  nor  $q_i = q_i^{\max} - tol_i^{hi}$ .

*Example 2.* Using the specifications for  $q_1$  in Example 1, the trajectory of  $d \dot{q}_1^* / d q_1$  versus  $q_1$  obtained by applying eqs. (8) - (10) is shown in Figure 2. The discontinuities are obvious. To alleviate this deficiency, a second algorithm for calculating the corrective action is discussed next.

### 3.2 Cycloidal Function Method

A second method is presented for calculating function  $\dot{q}_i^*$  such that it is sectionally smooth, uniformly continuous, and pointwise differentiable { with respect to  $q_i$  } throughout the entire range of joint  $i$ . Suppose  $\dot{q}_i^*$  is calculated for each and every joint  $i$  ( $= 1, 2, \dots, N$ ) based on the following conditional algorithm:

$$q_i^{\min} \leq q_i \leq (q_i^{\min} + tol_i^{lo}) : \quad \dot{q}_i^* = \frac{z_i \dot{q}_i^{\max}}{2\pi} \left\{ \frac{2\pi}{tol_i^{lo}} (q_i^{\min} + tol_i^{lo} - q_i) - \sin \left( \frac{2\pi}{tol_i^{lo}} (q_i^{\min} + tol_i^{lo} - q_i) \right) \right\} \quad (11)$$

$(q_i^{min} + tol_i^{lo}) < q_i < (q_i^{max} - tol_i^{hi})$  : Calculate  $\dot{q}_i^*$  by eq. (5)

$(q_i^{max} - tol_i^{hi}) \leq q_i \leq q_i^{max}$  :

$$\dot{q}_i^* = \frac{z_i \dot{q}_i^{max}}{2\pi} \left\{ \frac{2\pi}{tol_i^{hi}} (q_i^{max} - tol_i^{hi} - q_i) - \sin \left( \frac{2\pi}{tol_i^{hi}} (q_i^{max} - tol_i^{hi} - q_i) \right) \right\} \quad (12)$$

where, here again, it is assumed that  $tol_i^{hi} > 0$  and  $tol_i^{lo} > 0$ . In eqs. (11) and (12),  $\dot{q}_i^*$  has been defined by cycloidal functions [10]. Their use here is motivated in part by the fact the cycloidal functions are differentiable on all points and uniformly continuous, and the functions obtained by successively differentiating a cycloidal function are also differentiable on all points and uniformly continuous. Cycloidal functions have been applied to overcome the infinite jerk problem in the design and motion of cams [10]. They have also been previously used in a robotics context in [11] to generate reference trajectories for the joints of a manipulator.

To gain further insight into the benefits of defining  $\dot{q}_i^*$  by a cycloidal function, the first and second derivatives of eqs. (11) and (12) with respect to  $q_i$  are obtained:

$q_i^{min} \leq q_i \leq (q_i^{min} + tol_i^{lo})$  :

$$\frac{d\dot{q}_i^*}{dq_i} = -\frac{z_i \dot{q}_i^{max}}{tol_i^{lo}} \left\{ 1 - \cos \left( \frac{2\pi}{tol_i^{lo}} (q_i^{min} + tol_i^{lo} - q_i) \right) \right\}, \quad (13)$$

$$\frac{d^2 \{\dot{q}_i^*\}}{d\{q_i\}^2} = \frac{2\pi z_i \dot{q}_i^{max}}{(tol_i^{lo})^2} \sin \left( \frac{2\pi}{tol_i^{lo}} (q_i^{min} + tol_i^{lo} - q_i) \right) \quad (14)$$

$(q_i^{min} + tol_i^{lo}) < q_i < (q_i^{max} - tol_i^{hi})$  : Calculate  $d\dot{q}_i^* / dq_i$  using eq. (9)

$$\frac{d^2 \{\dot{q}_i^*\}}{d\{q_i\}^2} = 0 \quad (15)$$

$(q_i^{max} - tol_i^{hi}) \leq q_i \leq q_i^{max}$  :

$$\frac{d\dot{q}_i^*}{dq_i} = -\frac{z_i \dot{q}_i^{max}}{tol_i^{hi}} \left\{ 1 - \cos \left( \frac{2\pi}{tol_i^{hi}} (q_i^{max} - tol_i^{hi} - q_i) \right) \right\}, \quad (16)$$

$$\frac{d^2 \{\dot{q}_i^*\}}{d\{q_i\}^2} = \frac{2\pi z_i \dot{q}_i^{max}}{(tol_i^{hi})^2} \sin \left( \frac{2\pi}{tol_i^{hi}} (q_i^{max} - tol_i^{hi} - q_i) \right) \quad (17)$$

Evaluating each of eqs. (13) and (14) at angles  $q_i = q_i^{min}$  and  $q_i = q_i^{min} + tol_i^{lo}$ , respectively, gives results equal to zero. Evaluating each of eqs. (16) and (17) at angles  $q_i = q_i^{max}$  and  $q_i = q_i^{max} - tol_i^{hi}$ , respectively, also gives results equal to zero. It is immediately evident that the functions  $\dot{q}_i^*$  and  $d\dot{q}_i^* / dq_i$  are pointwise

differentiable throughout the range of motion of joint  $i$ . It is helpful to illustrate the cycloidal function method via an example.

*Example 3.* Here we repeat Examples 1 and 2 but employ the cycloidal function method for determining the corrective action  $\dot{q}_1^*$  and its derivative  $d\dot{q}_1^*/dq_1$  as functions of  $q_1$ . The trajectories of  $\dot{q}_1^*$  versus  $q_1$  and  $d\dot{q}_1^*/dq_1$  versus  $q_1$  when  $q_1$  lies in the lower prohibitive subrange shown in Figures 3 and 4 are obtained by applying eqs. (11) and (13), respectively. Likewise, the trajectories of  $\dot{q}_1^*$  versus  $q_1$  and  $d\dot{q}_1^*/dq_1$  versus  $q_1$  when  $q_1$  lies in the upper prohibitive subrange shown in Figures 5 and 6 are obtained by applying eqs. (12) and (16), respectively.

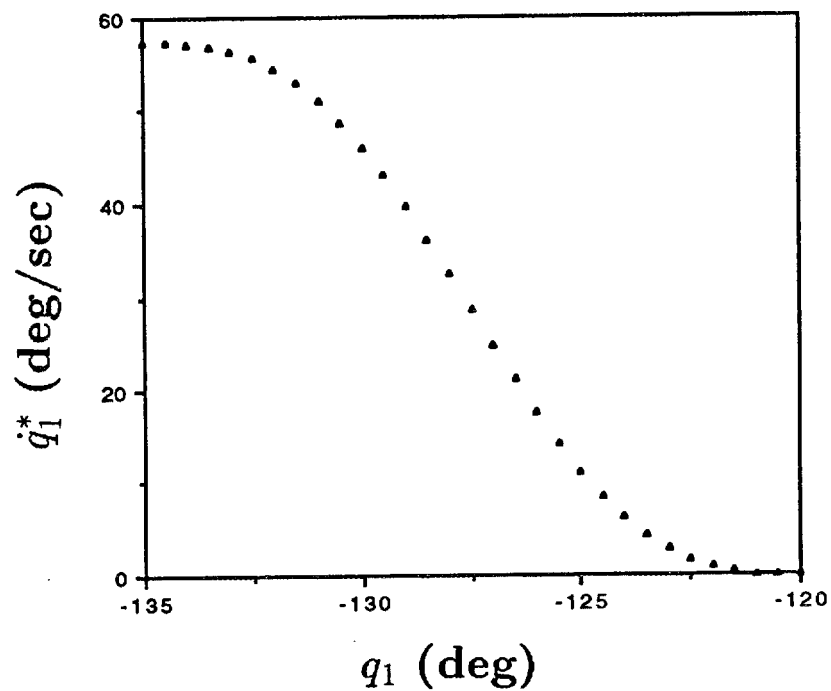


Figure 3. Trajectory of  $\dot{q}_1^*$  (Cycloidal Method)

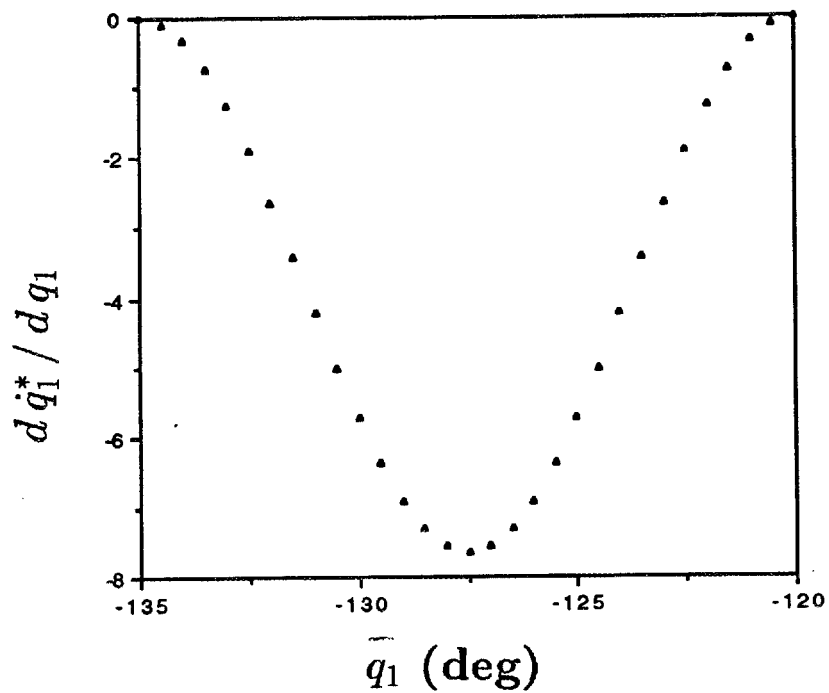


Figure 4. Trajectory of  $d\dot{q}_1^* / dq_1$  (Cycloidal Method)

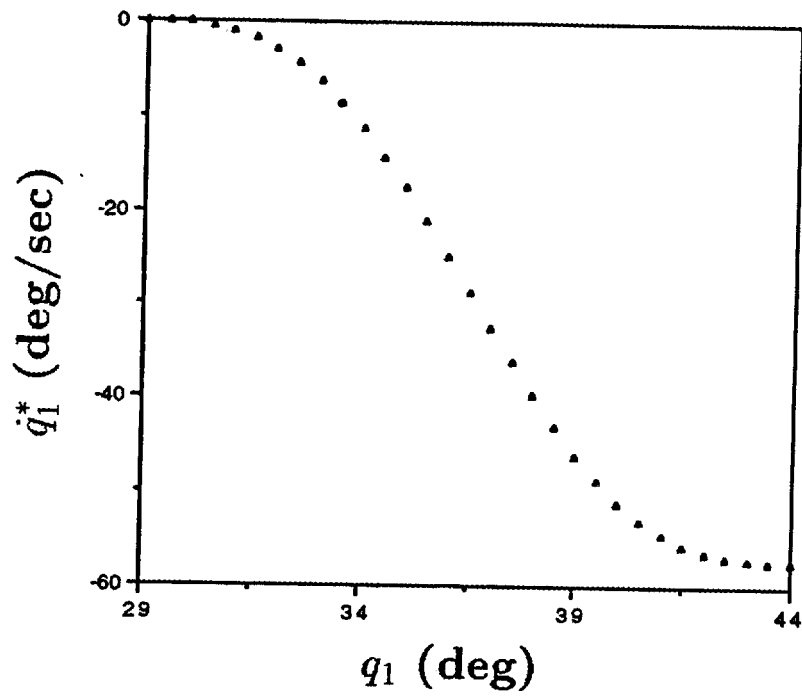


Figure 5. Trajectory of  $\dot{q}_1^*$  (Cycloidal Method)

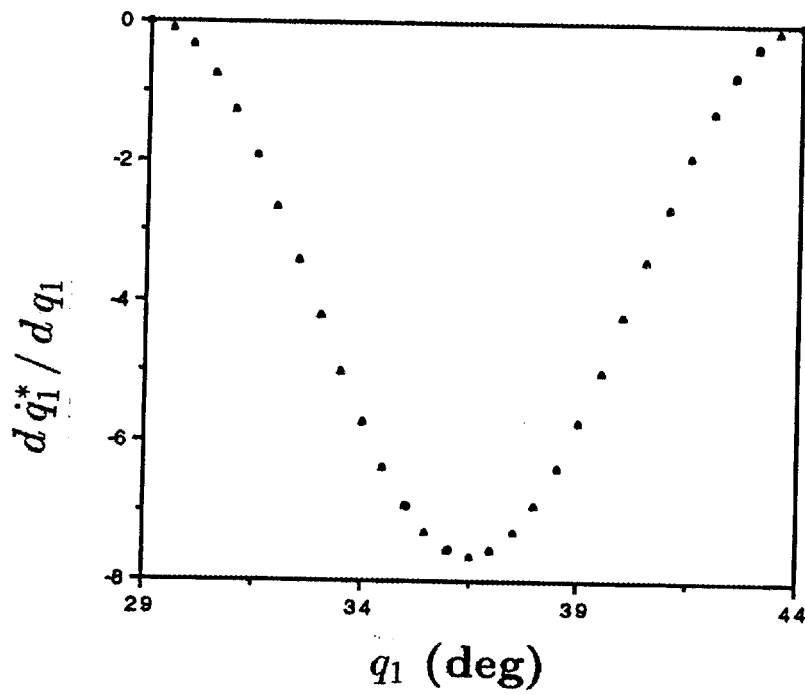


Figure 6. Trajectory of  $d\dot{q}_1^*/dq_1$  (Cycloidal Method)



## 4 Numerical Simulation Studies

The results of simulating the motion of a planar manipulator with four revolute joints using the two aforementioned joint limit avoidance (JLA) schemes are presented in this section. Only the translational motion of the tip of the manipulator is specified by the designer, so the system has two redundant degrees of freedom  $\{M = 2, N = 4\}$ . The link lengths  $l_i$  specified in meters are provided in Table 1:

LINK LENGTHS	
$i$	$l_i$
1	0.6096
2	0.6096
3	0.3048
4	0.3048

Table 1

The tip of the manipulator is commanded to move from point  $A$  to point  $B$  along a straight line, where the coordinates of the points are with respect to the base coordinate frame of the manipulator and are expressed in meters. The commanded trajectory has zero velocity and zero acceleration at the starting and ending points.

For each case study presented below, the joint trajectories resulting from simulating eq. (10)<sup>†</sup> with  $\dot{q}_i^*$  calculated three different ways are plotted on one set of axes: (a)  $\dot{q}_i^* = 0$  for all values of  $q_i$  ( $i = 1, 2, 3, 4$ ), which yields a minimum Euclidean norm solution for the joint velocities with no JLA; (b)  $\dot{q}_i^*$  is evaluated using eqs. (4) - (6) (linear function JLA method); and (c)  $\dot{q}_i^*$  is evaluated using eqs. (5), (11), and (12) (cycloidal function JLA method). The "fan" plots showing the manipulator's configuration during its motion when  $\dot{q}_i^*$  is calculated by each of the three ways are also presented.

*Case 1.* Choose  $\{x_A, y_A\} = \{1.219, 0.6096\}$  and  $\{x_B, y_B\} = \{0.6096, 0.6096\}$ . The total time to move from  $A$  to  $B$  is six seconds. The values specified for the quantities  $\{q_i^{max}, tol_i^{hi}, q_i^{min}, tol_i^{lo}, \dot{q}_i^{max}, z_i, q_i(A)\}$  are shown in Table 2, where  $q_i(A)$  signifies the values of joint  $i$  at point  $A$  and where all angular quantities are expressed in degrees or degrees per second:

CASE 1 PARAMETERS							
$i$	$q_i^{max}$	$tol_i^{hi}$	$q_i^{min}$	$tol_i^{lo}$	$\dot{q}_i^{max}$	$z_i$	$q_i(A)$
1	145.0	10.0	-145.0	10.0	57.296	1.0	90.0
2	145.0	10.0	-145.0	10.0	57.296	1.0	-90.0
3	145.0	10.0	-145.0	10.0	57.296	1.0	0.0
4	145.0	10.0	-145.0	10.0	57.296	1.0	0.0

Table 2

The manipulator "fan" plots when  $\dot{q}_i^*$  is calculated by each of the three aforementioned ways are shown in Figures 1.F1-1.F3, respectively. The trajectories of the joints are shown in Figures 1.J1A-B through 1.J4A-B, where the plot notation  $q_i(\text{no\_jla})$  denotes the trajectory of  $q_i$  when there is no JLA algorithm active at any time, and where  $q_i(\text{jla})$  and  $q_i(\text{jla\_cyc})$  signify the trajectory of  $q_i$  when  $\dot{q}_i^*$  is calculated by the linear and cycloidal function JLA methods, respectively. The "B" figures highlight the portions of the "A" figures where the JLA algorithms become active.

Keeping in mind that a simulated manipulator is a fictitious entity, plots of the joint trajectories when no joint limit avoidance was active were made. Then, to test the effectiveness of the JLA algorithms in an extreme case, joint limit  $q_1^{max}$  was deliberately chosen such that  $q_1(\text{no\_jla})$  exceeded it over the range of motion of joint one. Of course,  $q_1$  cannot exceed  $q_1^{max}$  in a physical robot. Figures 1.J1A and 1.J1B reveal that the application of either JLA algorithm results in  $q_1$  no longer exceeding  $q_1^{max}$  and furthermore each method successfully moves joint one away from its upper limit. The trajectories of joints 2-4, which do not move into their respective prohibitive outer ranges, are shown in Figures 1.J2A-B through 1.J4A-B.

*Case 2.* The identical Cartesian trajectory is used, but now  $tol_i^{hi}$  and  $tol_i^{lo}$  are one-half of their values used in Case 1 (see Table 3):

CASE 2 PARAMETERS							
$i$	$q_i^{max}$	$tol_i^{hi}$	$q_i^{min}$	$tol_i^{lo}$	$\dot{q}_i^{max}$	$z_i$	$q_i(A)$
1	145.0	5.0	-145.0	5.0	57.296	1.0	90.0
2	145.0	5.0	-145.0	5.0	57.296	1.0	-90.0
3	145.0	5.0	-145.0	5.0	57.296	1.0	0.0
4	145.0	5.0	-145.0	5.0	57.296	1.0	0.0

Table 3

The fan plots when  $\dot{q}_i^*$  is calculated by each of the three aforementioned ways are shown in Figures 2.F1-2.F3, respectively. Observing Figures 2.J1A and 2.J1B reveal that both JLA algorithms again succeed in preventing  $q_1$  from exceeding its upper range limit and move it away from the limit. None of the other joints move within their prohibitive regions, and their trajectories are plotted in Figures 2.J2A-B through 2.J4A-B.

*Case 3.* The identical Cartesian trajectory specified in Case 1 is used, but the scaled peak velocity  $(z_i \dot{q}_i^{max}), i = 1, 2, 3, 4$  is reduced to one-half of its peak value used in Case 1 (see Table 4):

CASE 3 PARAMETERS							
$i$	$q_i^{max}$	$tol_i^{hi}$	$q_i^{min}$	$tol_i^{lo}$	$\dot{q}_i^{max}$	$z_i$	$q_i(A)$
1	145.0	10.0	-145.0	10.0	57.296	0.5	90.0
2	145.0	10.0	-145.0	10.0	57.296	0.5	-90.0
3	145.0	10.0	-145.0	10.0	57.296	0.5	0.0
4	145.0	10.0	-145.0	10.0	57.296	0.5	0.0

Table 4

The fan plots when  $\dot{q}_i^*$  is calculated by each of the three aforementioned ways are shown in Figures 3.F1-3.F3, respectively. Observing Figures 3.J1A and 3.J1B reveal that both JLA algorithms again succeed in preventing  $q_1$  from exceeding its upper range limit and move it away from the limit. None of the other joints move within their prohibitive regions, and their trajectories are plotted in Figures 3.J2A-B through 3.J4A-B.

*Case 4.* In each of the previous cases, only joint one moved into a prohibitive outer range. Again using the identical end effector trajectory given in Case 1, we select values for the joint range limits and tolerances such that multiple joints move into their

respective prohibitive ranges simultaneously so as to check the effectiveness of the JLA algorithms. Specifically, we select values for the quantities  $\{q_1^{max}, tol_1^{hi}, q_3^{min}, tol_3^{lo}\}$  such that joints one and three pass into their upper and lower prohibitive ranges of motion simultaneously. The decision to choose joint three is motivated by the fact that when only joint one moved into its upper prohibitive range (i.e., as in Case 1),  $q_3(jla)$  and  $q_3(jla\_cyc)$  decreased more rapidly than  $q_3(no\_jla)$  (see Figure 1.J3B). Here  $q_3(jla)$  and  $q_3(jla\_cyc)$  are expected to increase in value when joint three moves into its lower prohibitive region. The values of the parameters used in Case 4 are provided in Table 5:

CASE 4 PARAMETERS							
$i$	$q_i^{max}$	$tol_i^{hi}$	$q_i^{min}$	$tol_i^{lo}$	$\dot{q}_i^{max}$	$z_i$	$q_i(A)$
1	150.0	10.0	-150.0	10.0	57.296	1.0	90.0
2	150.0	10.0	-150.0	10.0	57.296	1.0	-90.0
3	150.0	10.0	-30.0	10.0	57.296	1.0	0.0
4	150.0	10.0	-150.0	10.0	57.296	1.0	0.0

Table 5

The fan plots are shown in Figures 4.F1-4.F3. The joint trajectories are plotted in Figures 4.J1A-B through 4.J4A-B. At  $t = 4.088$  seconds joint three falls into its lower prohibitive range and the JLA algorithms are activated. Then at  $t = 4.256$  seconds joint one moves into its upper prohibitive range. Figures 4.J1A-B and 4.J3A-B reveal that both JLA algorithms successfully move joints one and three back towards their respective centermost ranges.

*Case 5.* To further observe the behavior of the manipulator when multiple joints move within their prohibitive outer ranges, we repeat Case 4, but increase the lower range limit for joint three from  $-30^\circ$  (the value used in Case 4) to  $-26^\circ$ . Now  $q_3(no\_jla)$  is in very close proximity to its lower limit  $q_3^{min}$  (see Figure 5.J3B). The parameter settings are provided in Table 6:

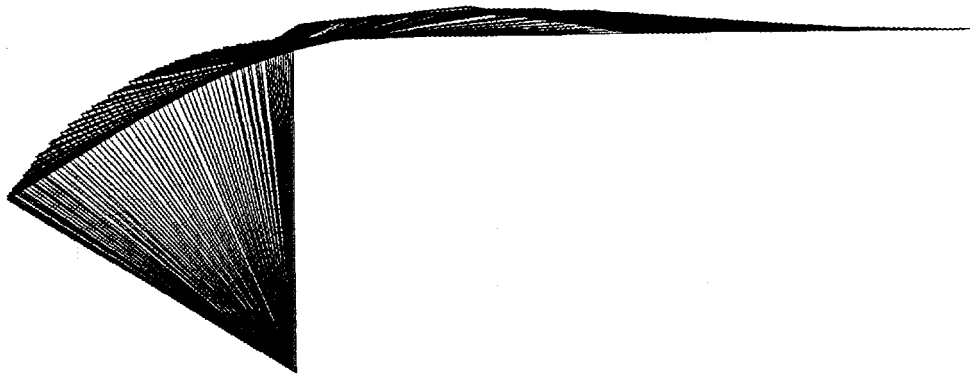
CASE 5 PARAMETERS							
$i$	$q_i^{max}$	$tol_i^{hi}$	$q_i^{min}$	$tol_i^{lo}$	$\dot{q}_i^{max}$	$z_i$	$q_i(A)$
1	150.0	10.0	-150.0	10.0	57.296	1.0	90.0
2	150.0	10.0	-150.0	10.0	57.296	1.0	-90.0
3	150.0	10.0	-26.0	10.0	57.296	1.0	0.0
4	150.0	10.0	-150.0	10.0	57.296	1.0	0.0

Table 6

The fan plots are given in Figures 5.F1-5.F3 and the the joint trajectories are plotted in Figures 5.J1A-B through 5.J4A-B. At  $t = 3.528$  seconds joint three moves into its lower prohibitive range and the JLA algorithms are activated. Then at  $t = 4.256$  seconds joint one moves into its upper prohibitive range. The moment when both joints are in their prohibitive ranges simultaneously appears to be noticeable in Figure 5.J3B where  $q_3(jla)$  and  $q_3(jla\_cyc)$  first incrementally decrease then begin increasing as anticipated. The time interval where  $q_3(jla)$  and  $q_3(jla\_cyc)$  decrease is viewed as a transient period. Figure 5.J1B shows that both JLA algorithms successfully move joint one away from its upper limit.

The results of the numerical experiments do not indicate a significant difference in the performances of the linear and cycloidal function joint limit avoidance algorithms.

**FIGURES**  
**FOR**  
**CASE ONE**



**Figure 1.F1 Fan Plot With No JLA (Case 1)**

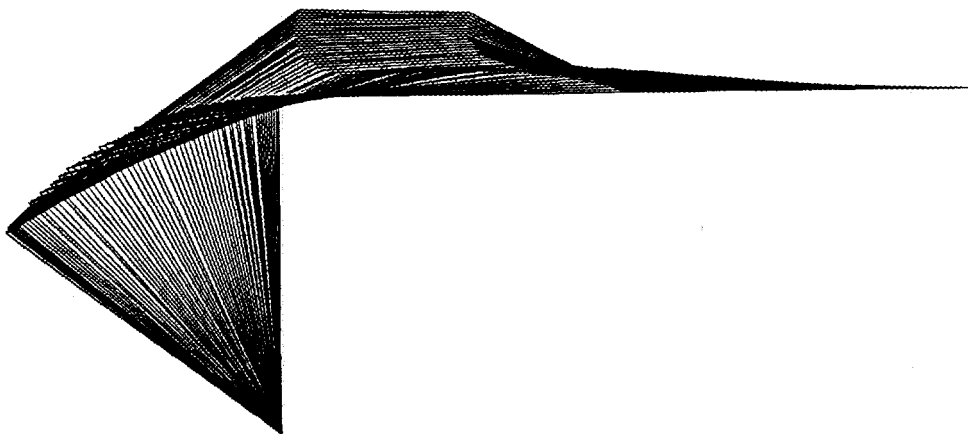


**Figure 1.F2 Fan Plot Using Linear JLA Method**

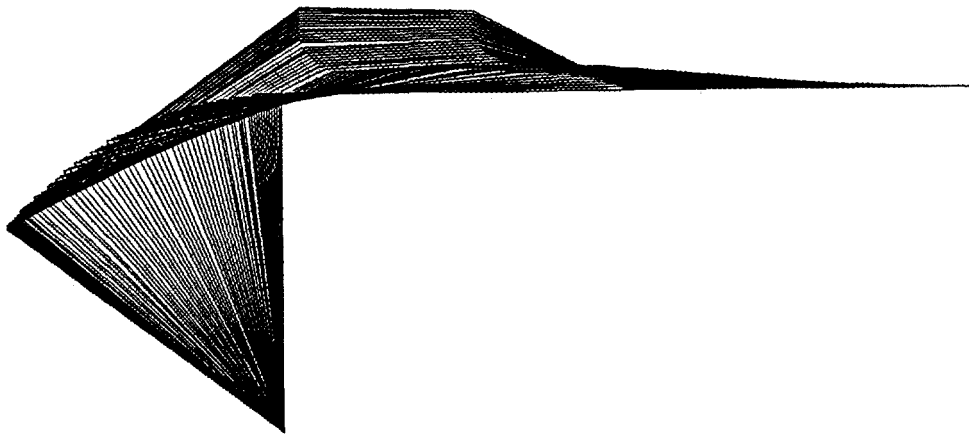


**Figure 1.F3 Fan Plot Using Cycloidal JLA Method**

### CASE 1

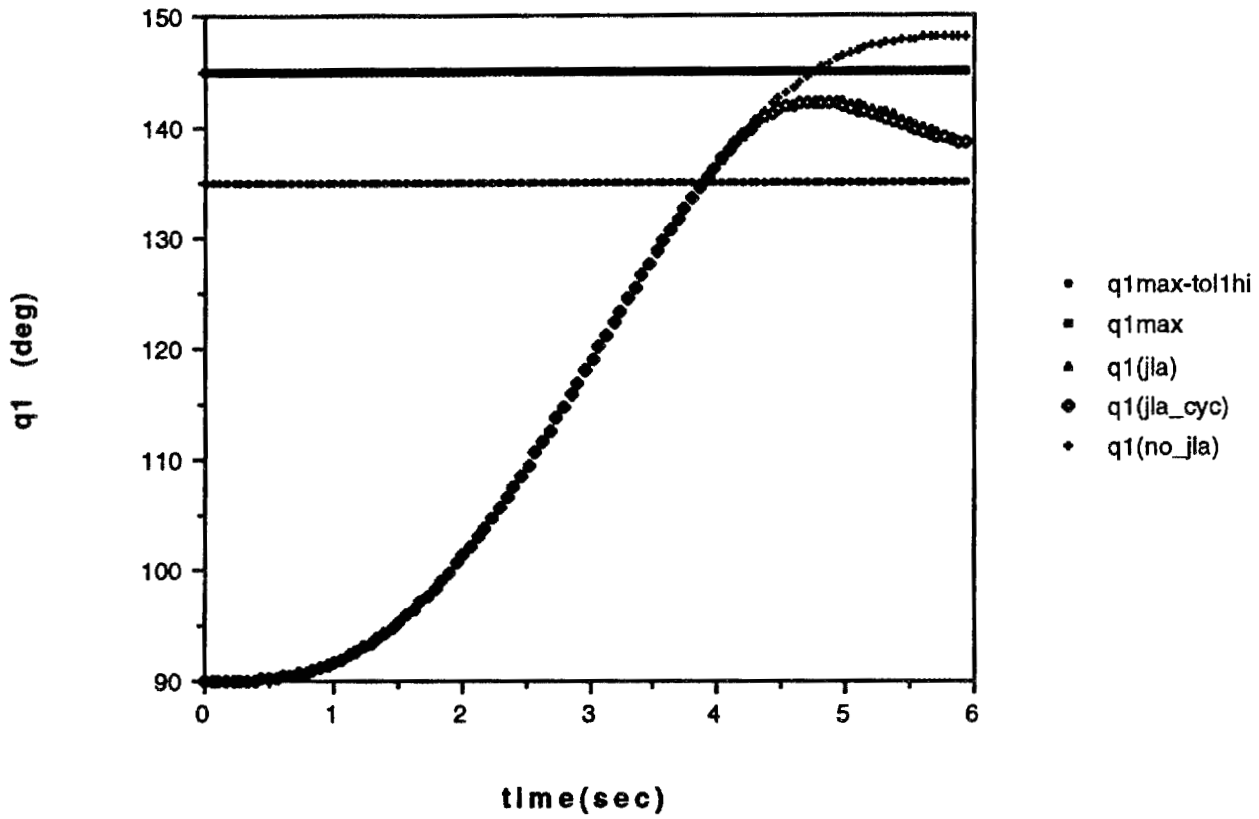


Figure 1.J1A Trajectories for Joint One (Entire Range of Motion)

### CASE 1

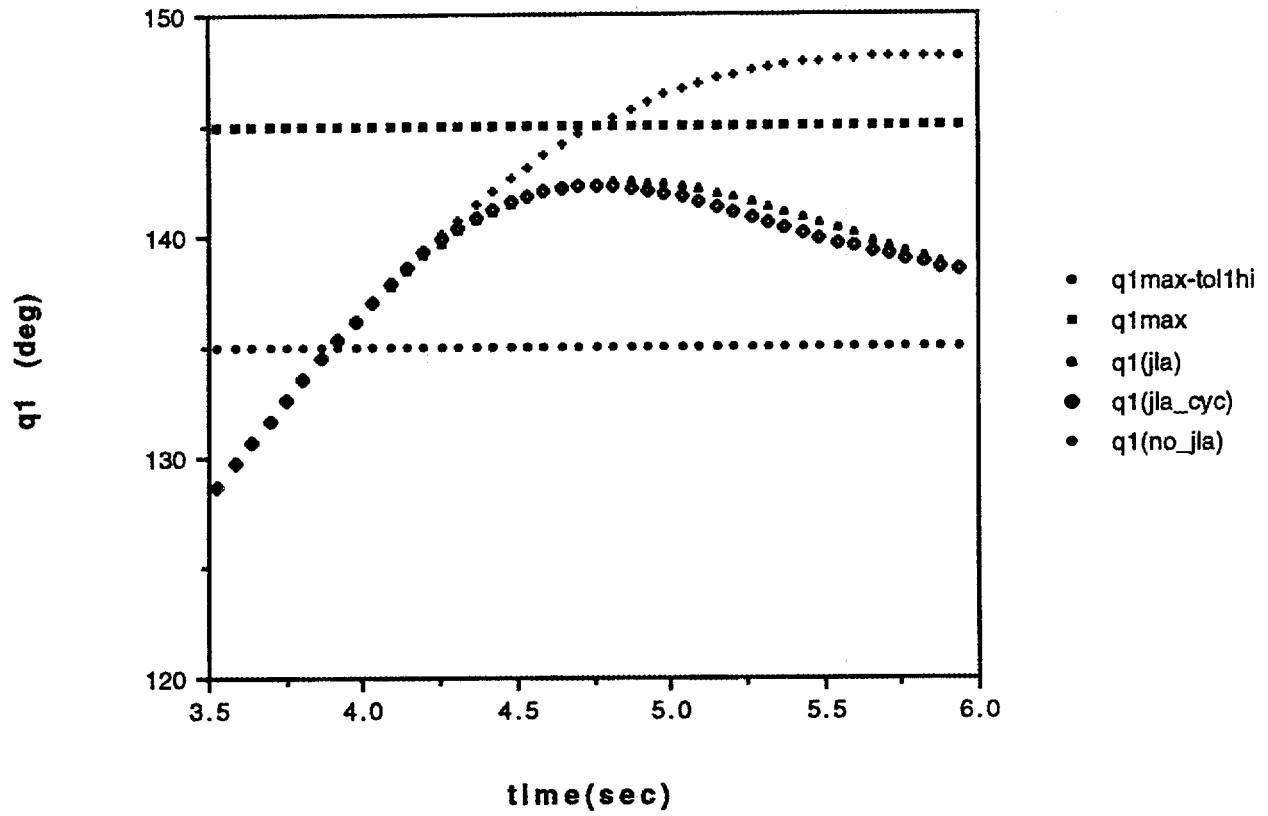


Figure 1.J1B Trajectories for Joint One (Range Where JLA is Active)

### CASE 1

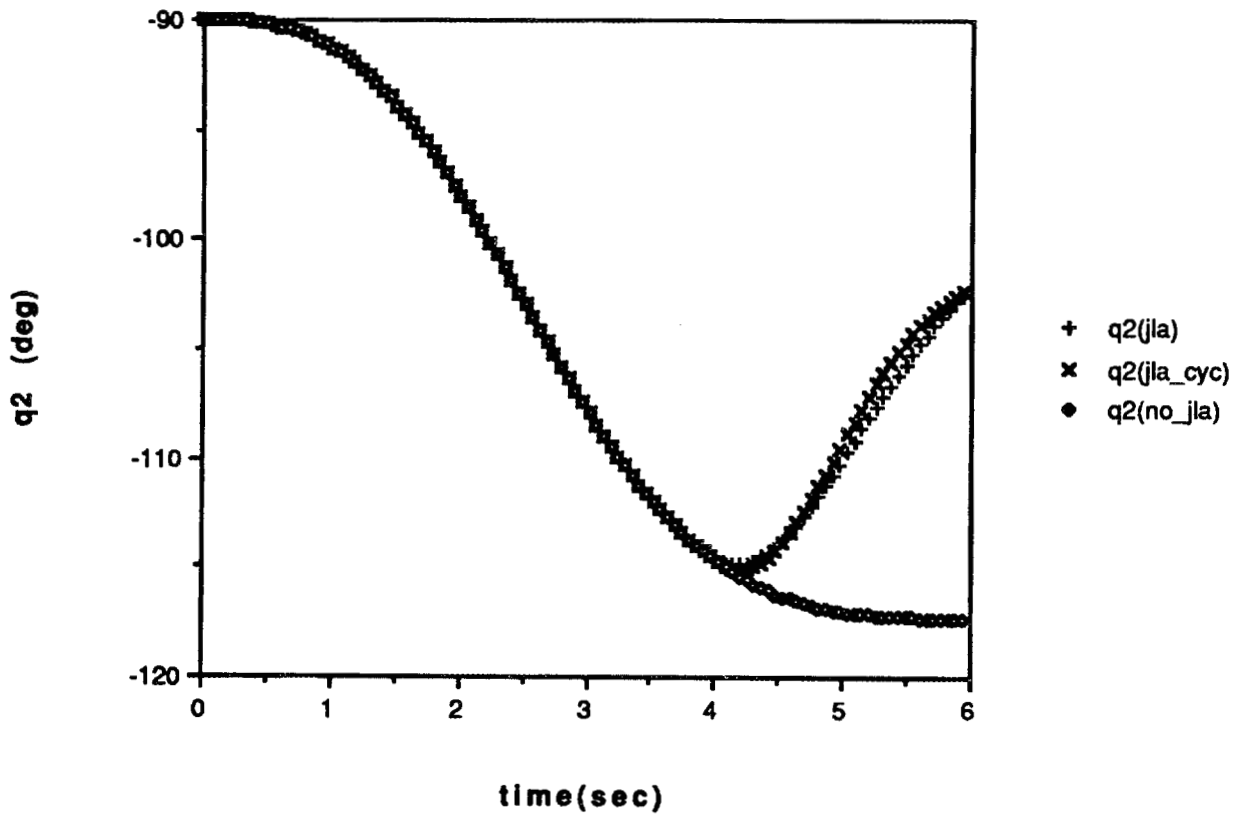


Figure 1.J2A Trajectories for Joint Two (Entire Range of Motion)

### CASE 1

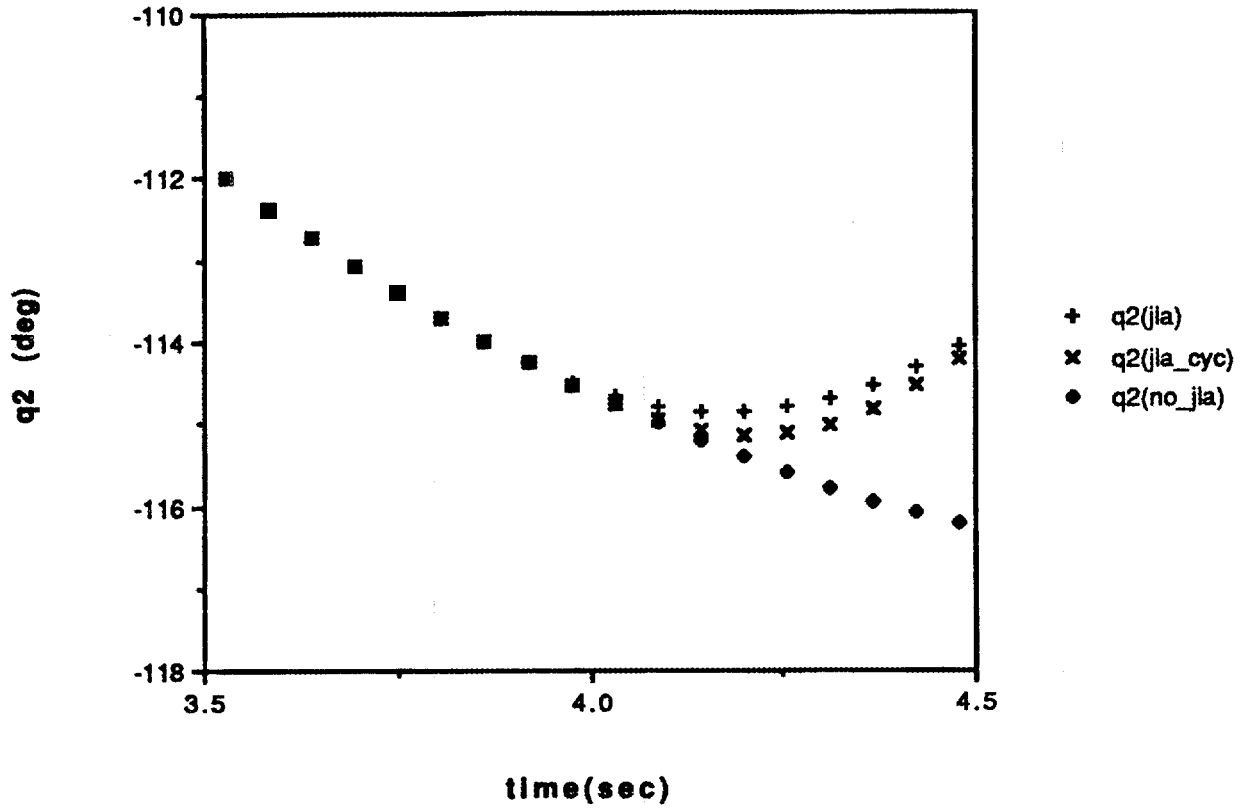


Figure 1.J2B Trajectories for Joint Two (Range Where JLA is Active)

### CASE 1

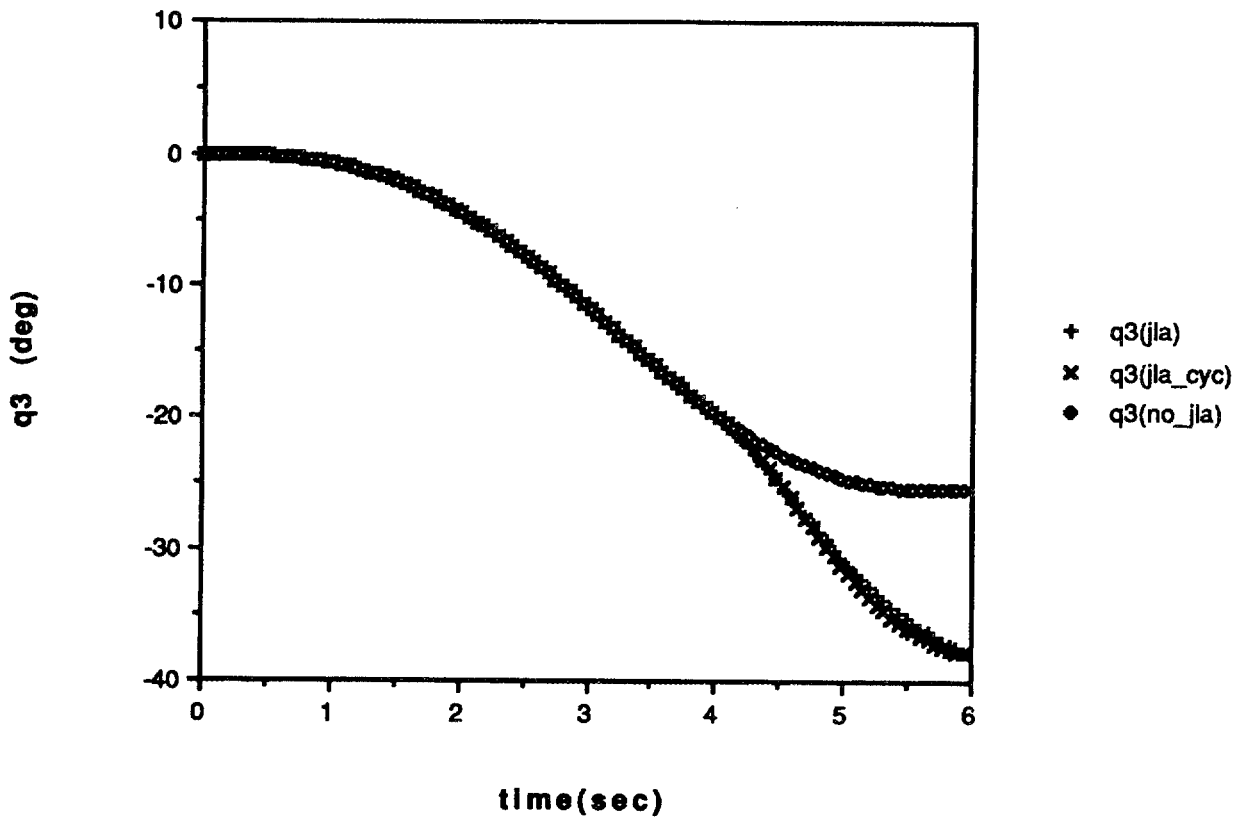


Figure 1.J3A Trajectories for Joint Three (Entire Range of Motion)

### CASE 1

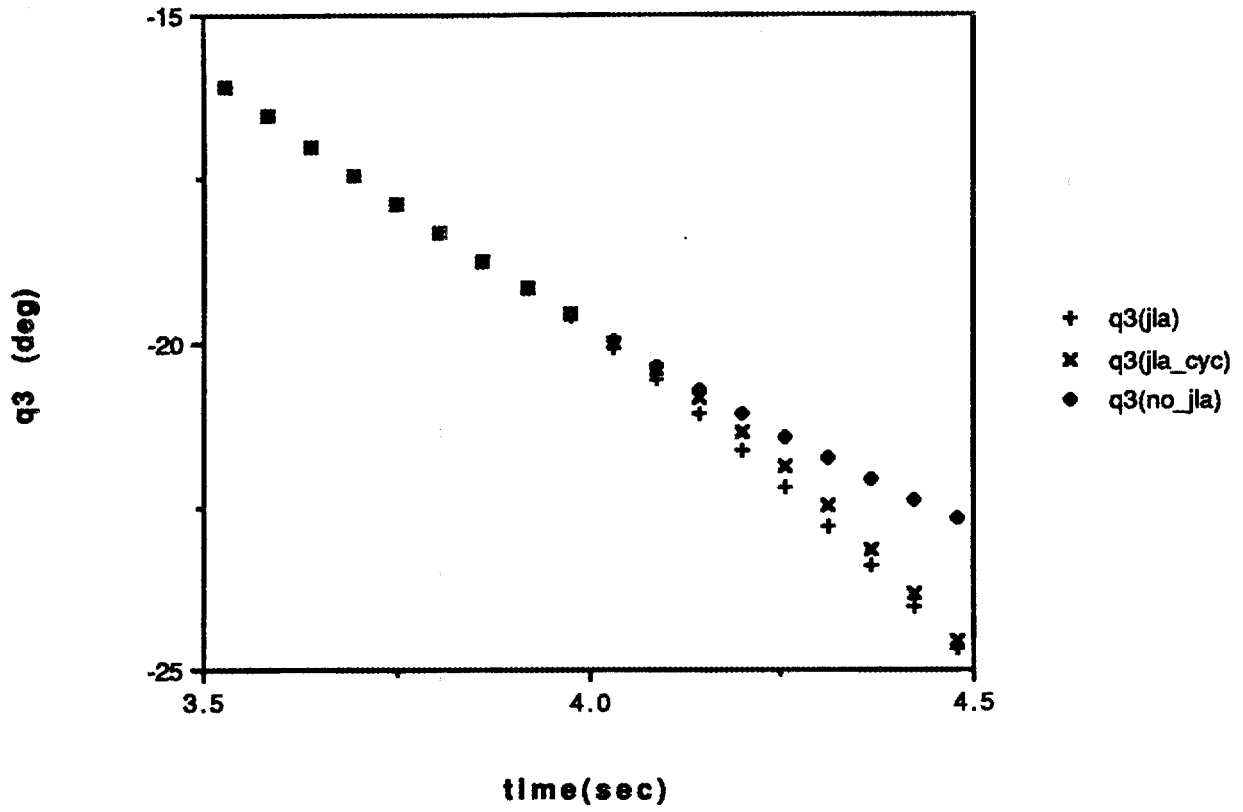


Figure 1.J3B Trajectories for Joint Three (Range Where JLA is Active)

### CASE 1

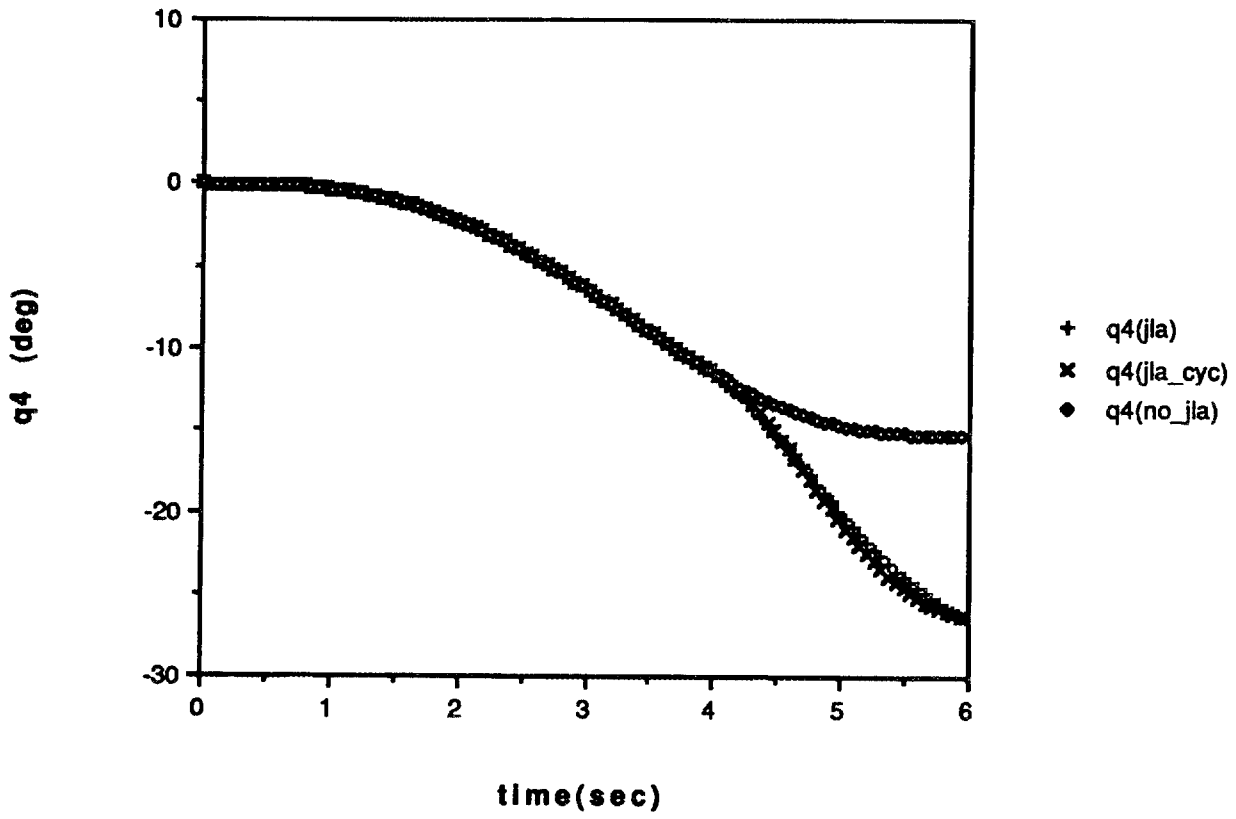


Figure 1.J4A Trajectories for Joint Four (Entire Range of Motion)

### CASE 1

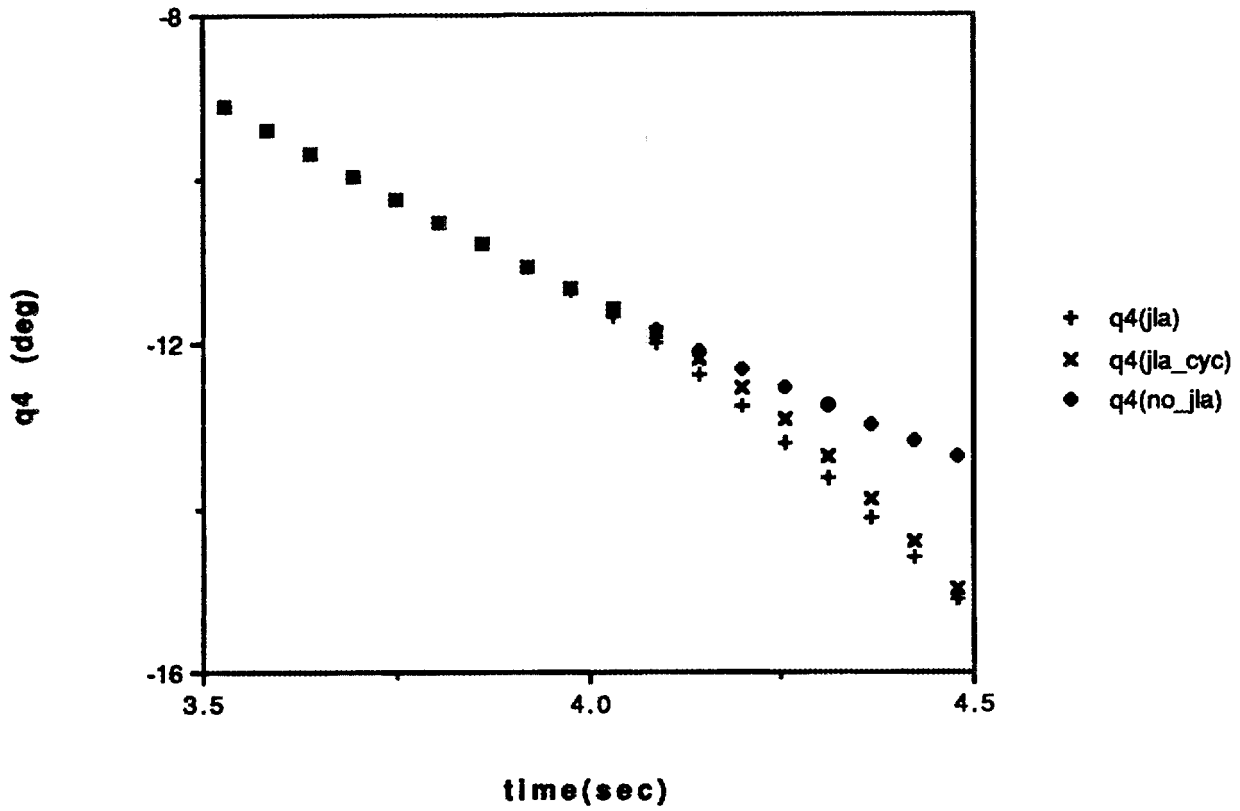
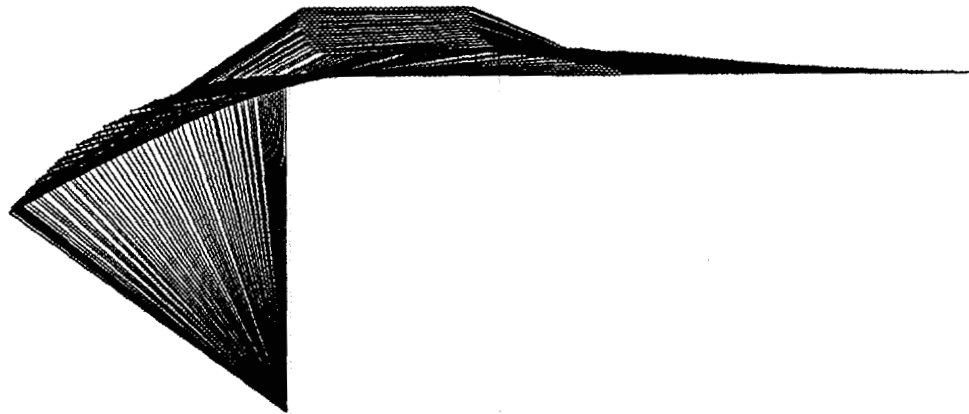


Figure 1.J4B Trajectories for Joint Four (Range Where JLA is Active)

**FIGURES**  
**FOR**  
**CASE TWO**



**Figure 2.F1 Fan Plot With No JLA (Case 2)**



**Figure 2.F2 Fan Plot Using Linear JLA Method**

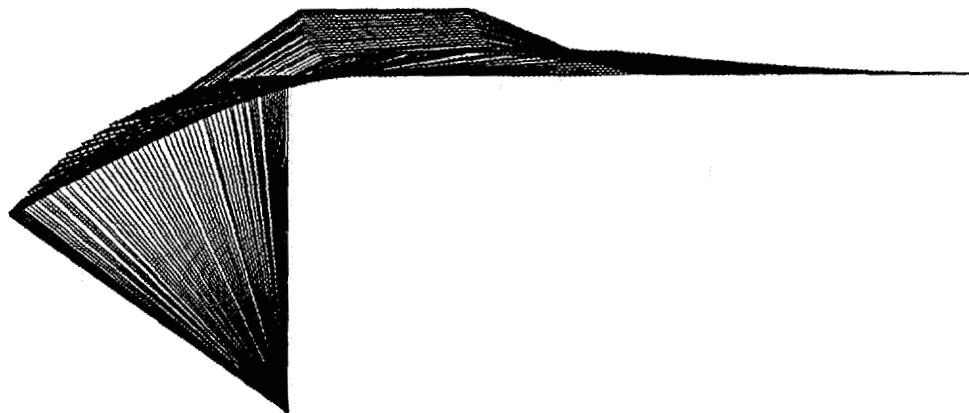


**Figure 2.F3 Fan Plot Using Cycloidal JLA Method**

### CASE 2

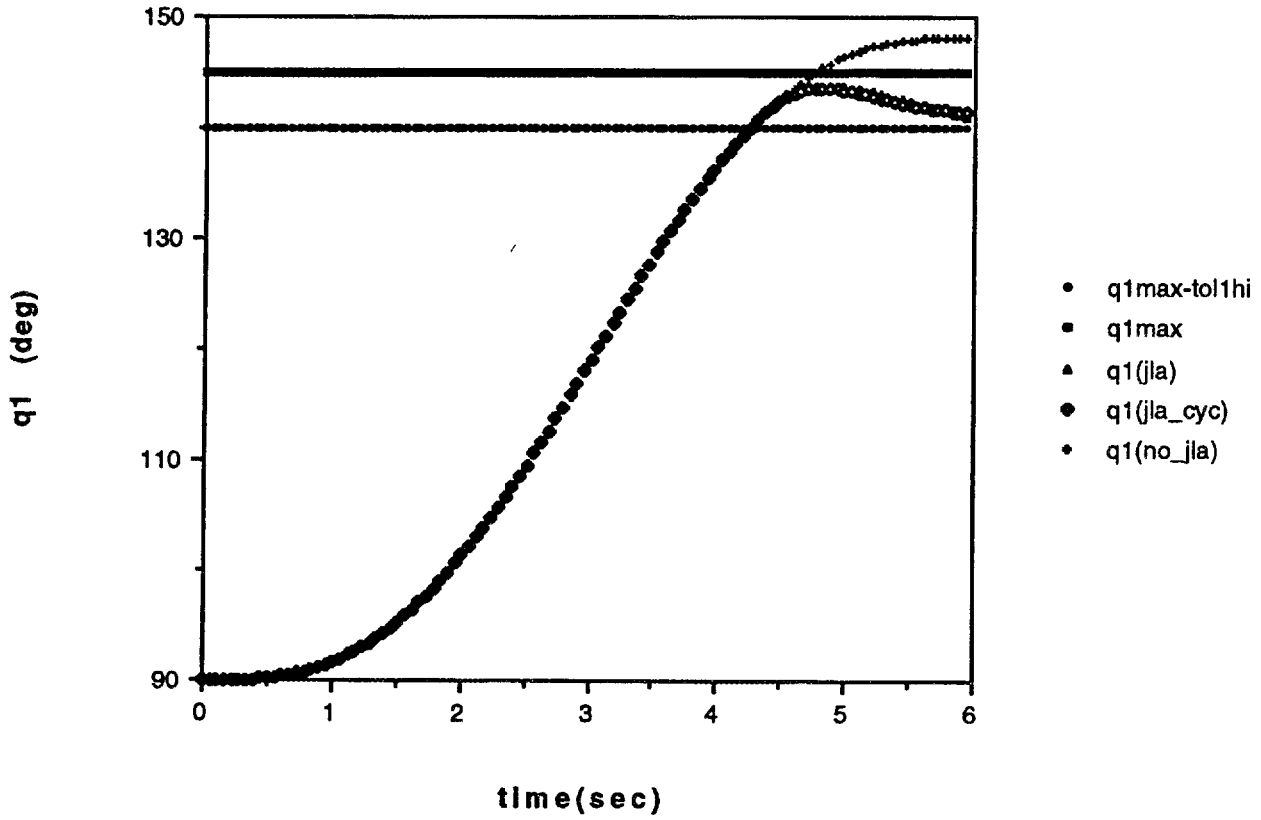


Figure 2.J1A Trajectories for Joint One (Entire Range of Motion)

### CASE 2

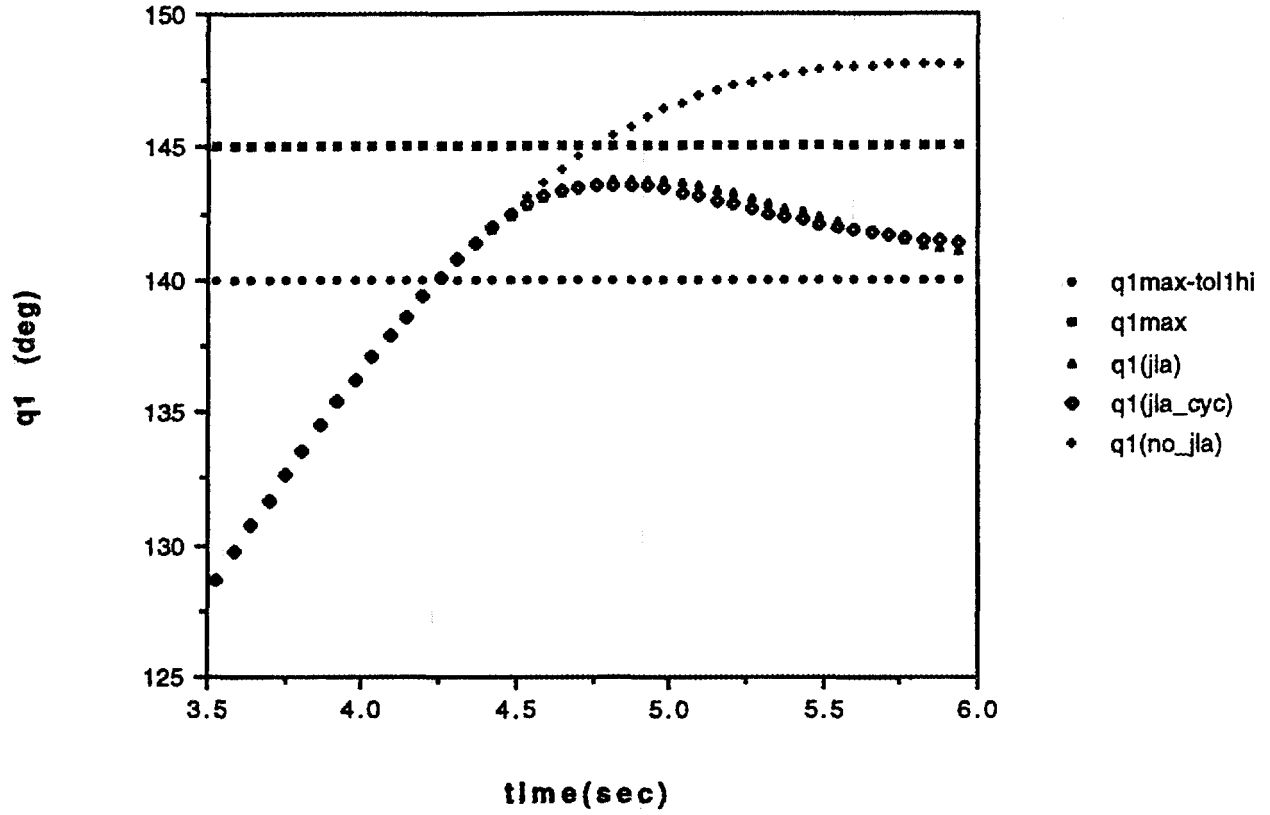


Figure 2.J1B Trajectories for Joint One (Range Where JLA is Active)

### CASE 2

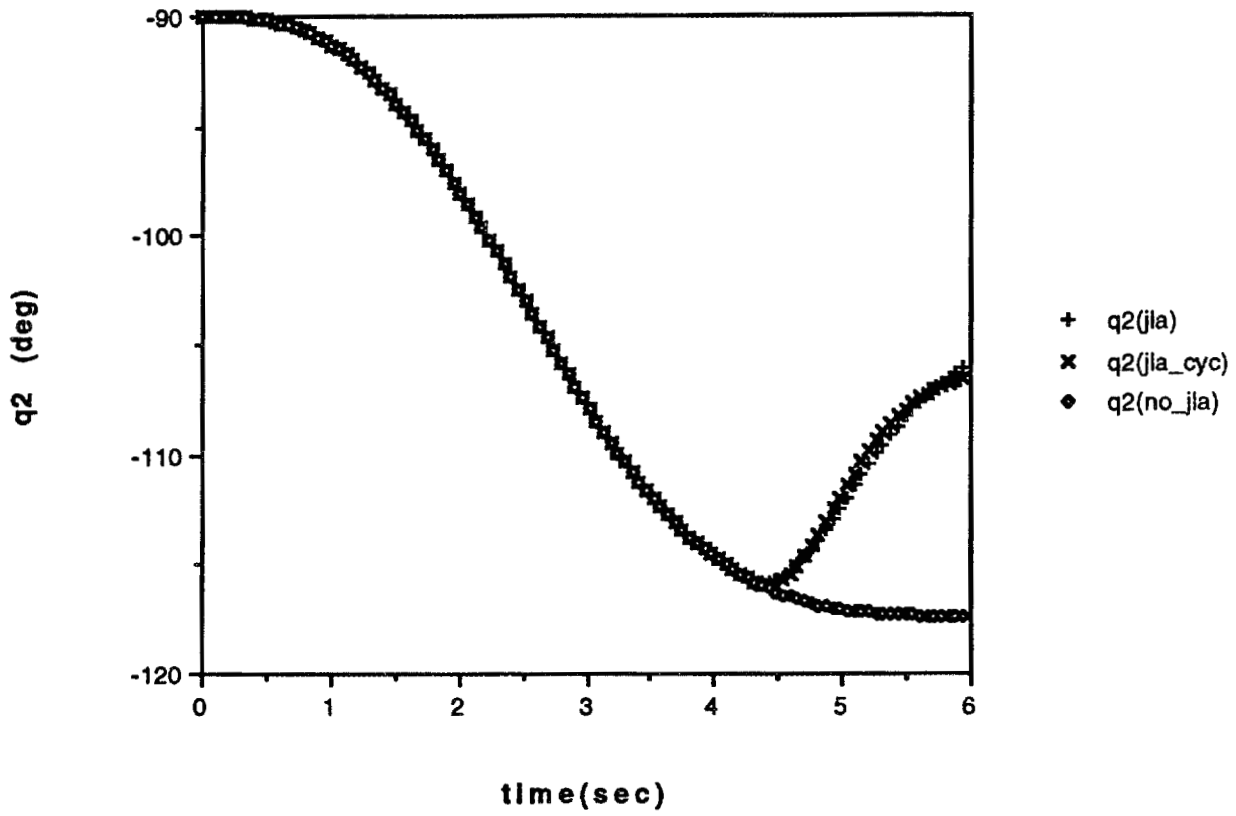


Figure 2.J2A Trajectories for Joint Two (Entire Range of Motion)

### CASE 2

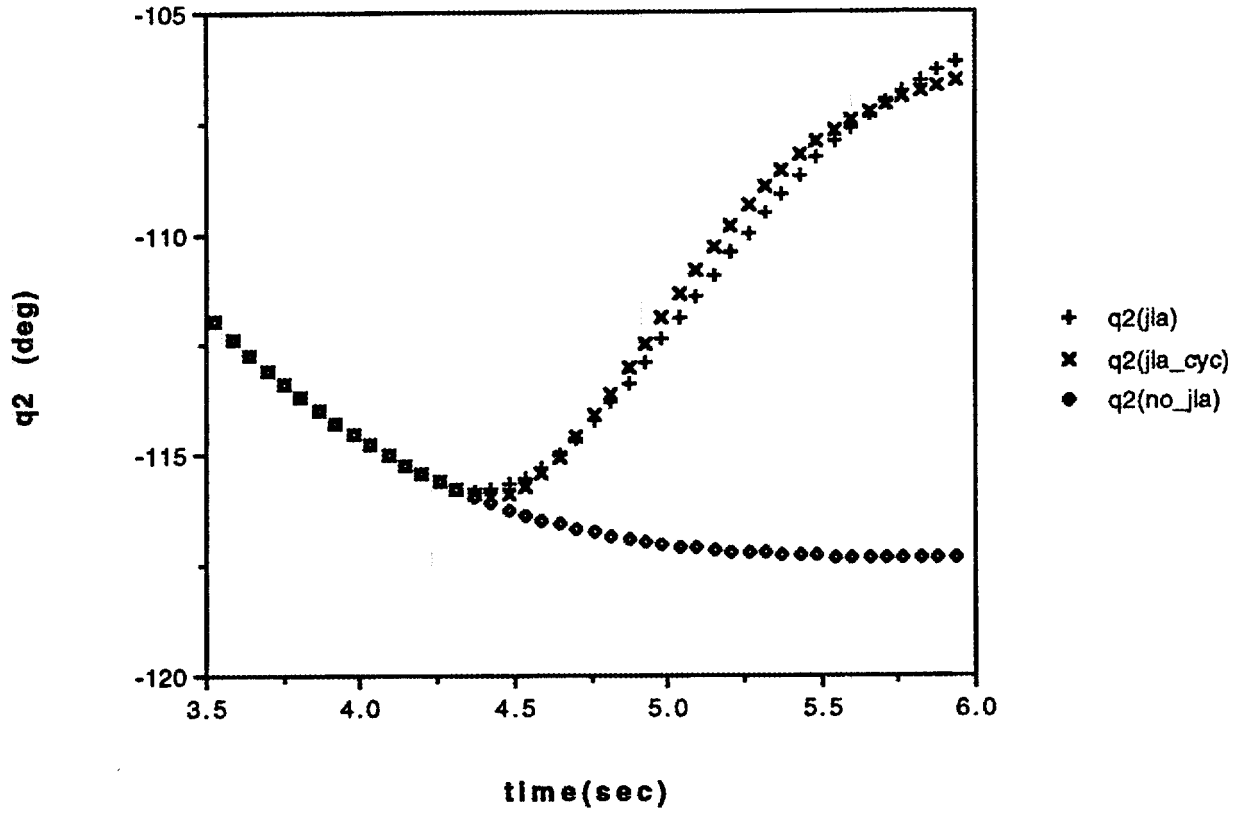


Figure 2.J2B Trajectories for Joint Two (Range Where JLA is Active)

### CASE 2

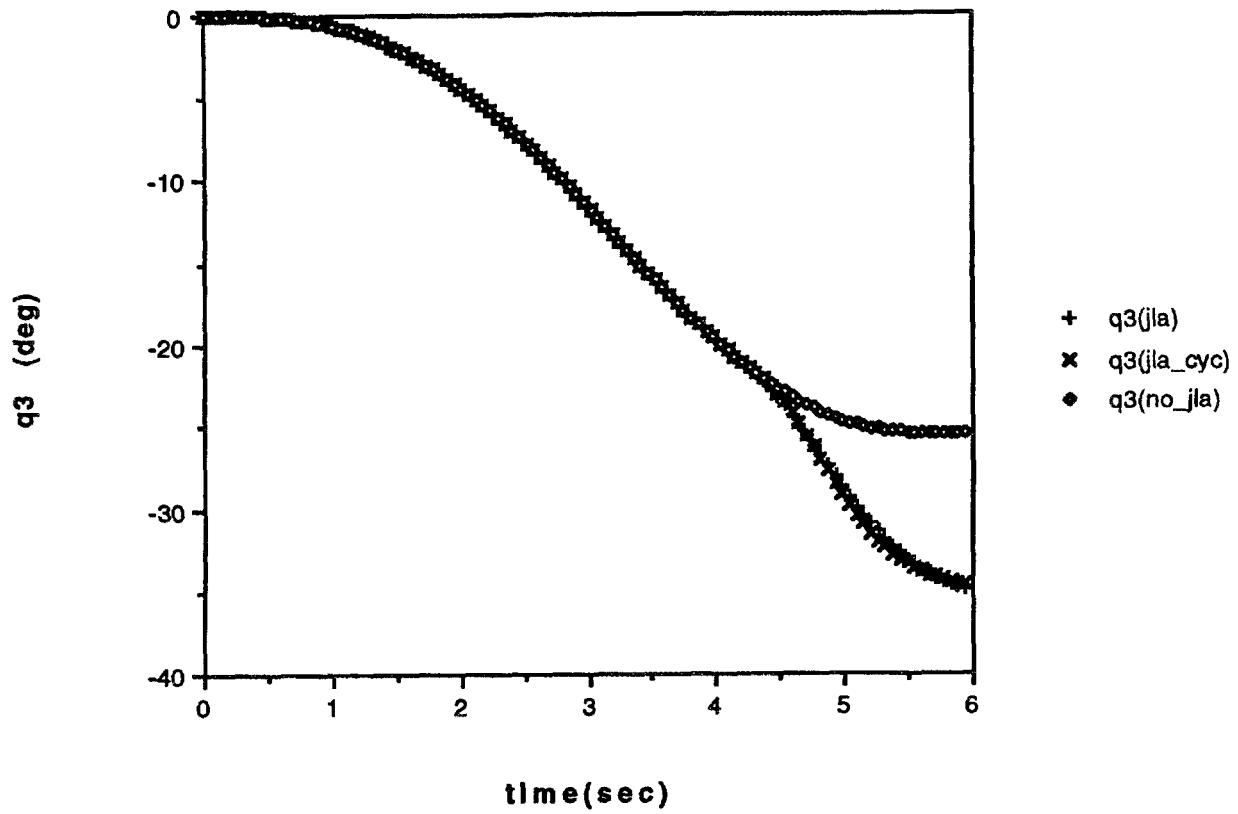


Figure 2.J3A Trajectories for Joint Three (Entire Range of Motion)

### CASE 2

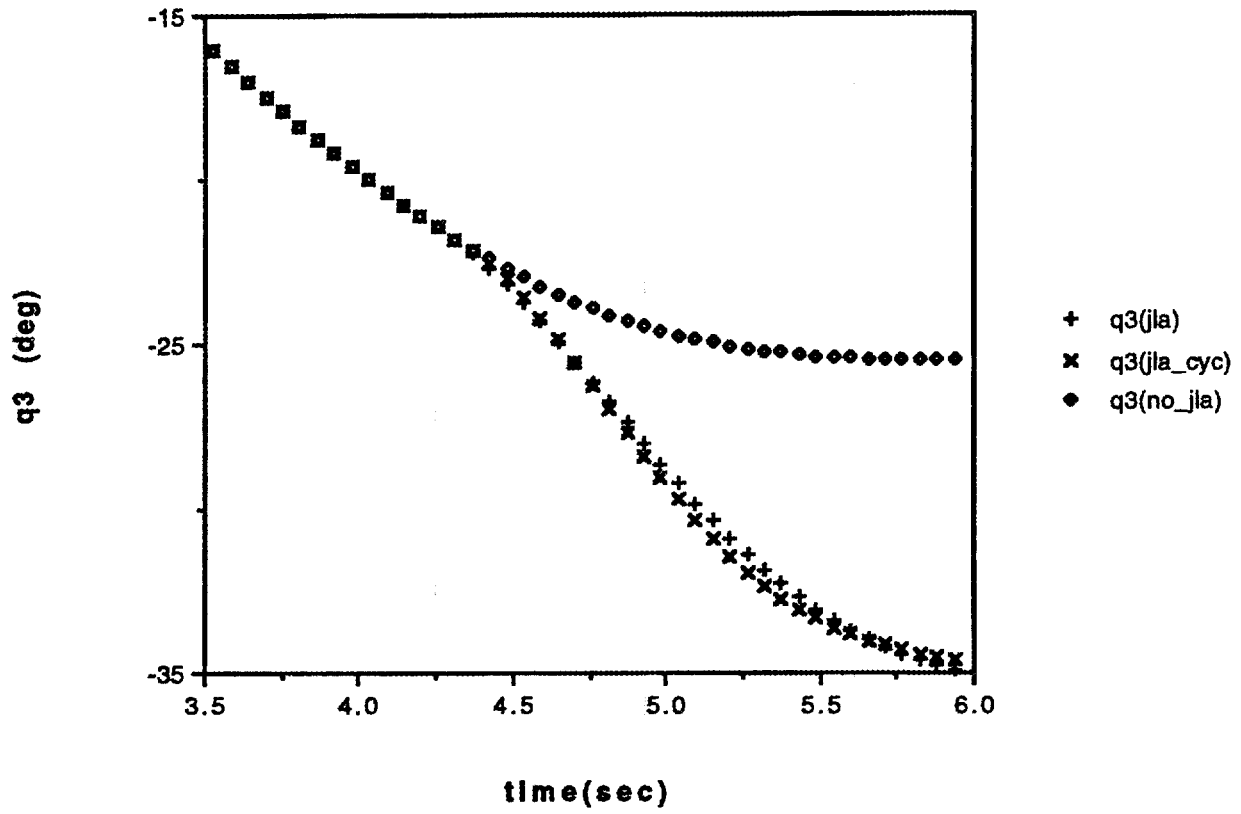


Figure 2.J3B Trajectories for Joint Three (Range Where JLA is Active)

### CASE 2

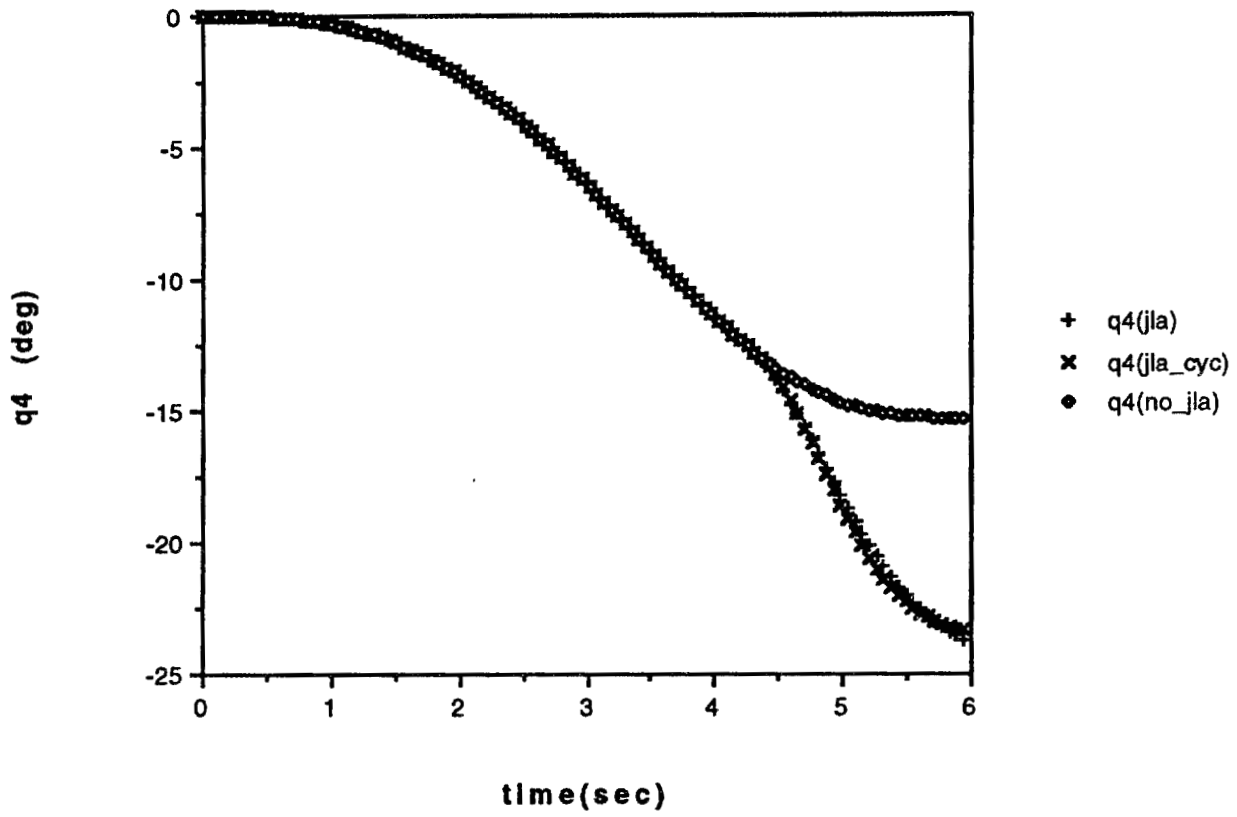


Figure 2.J4A Trajectories for Joint Four (Entire Range of Motion)

### CASE 2

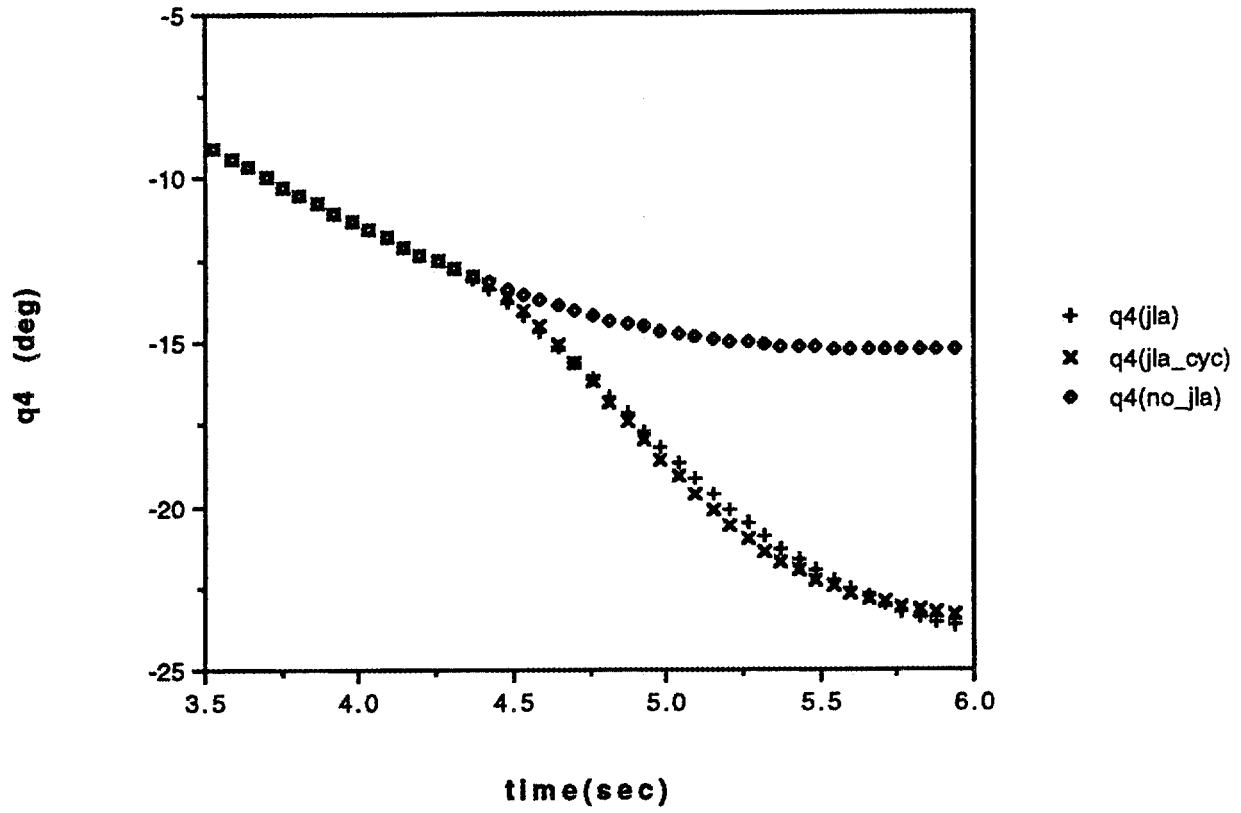
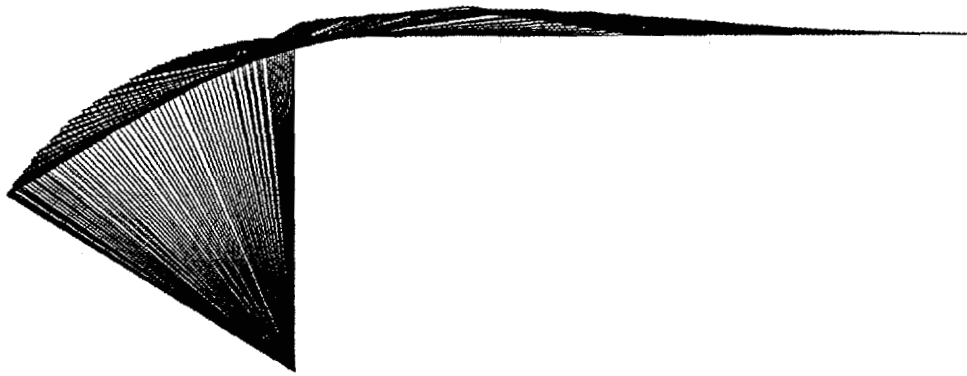
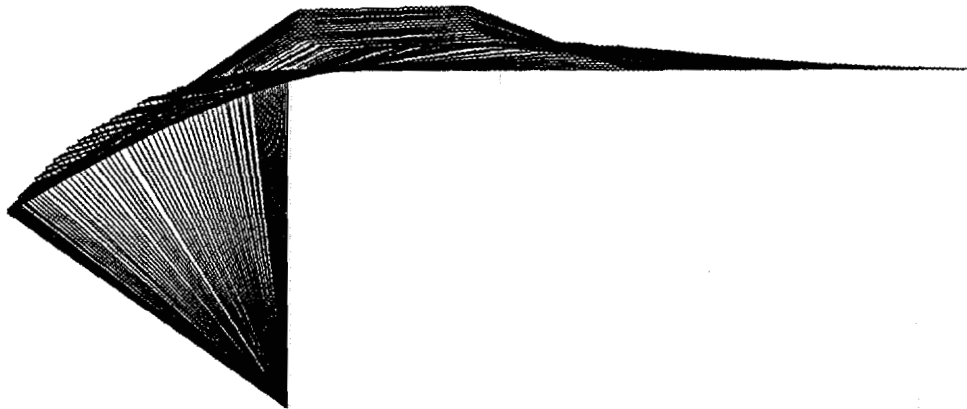


Figure 2.J4B Trajectories for Joint Four (Range Where JLA is Active)

**FIGURES**  
**FOR**  
**CASE THREE**



**Figure 3.F1 Fan Plot With No JLA (Case 3)**



**Figure 3.F2 Fan Plot Using Linear JLA Method**

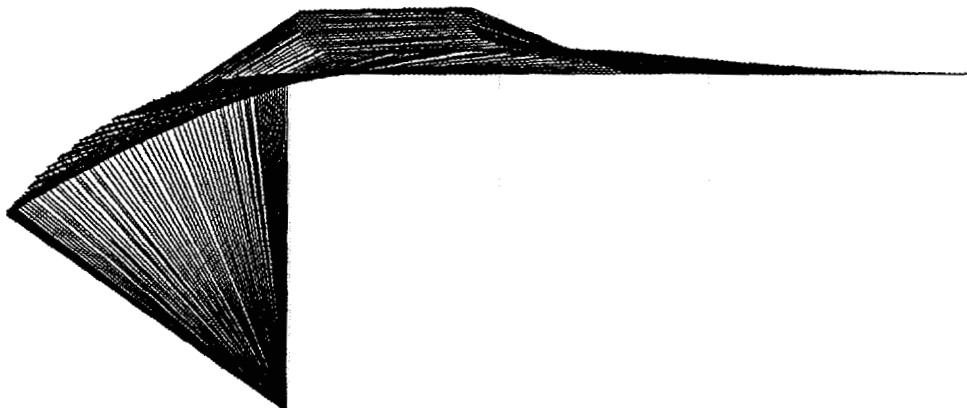


**Figure 3.F3 Fan Plot Using Cycloidal JLA Method**

### CASE 3

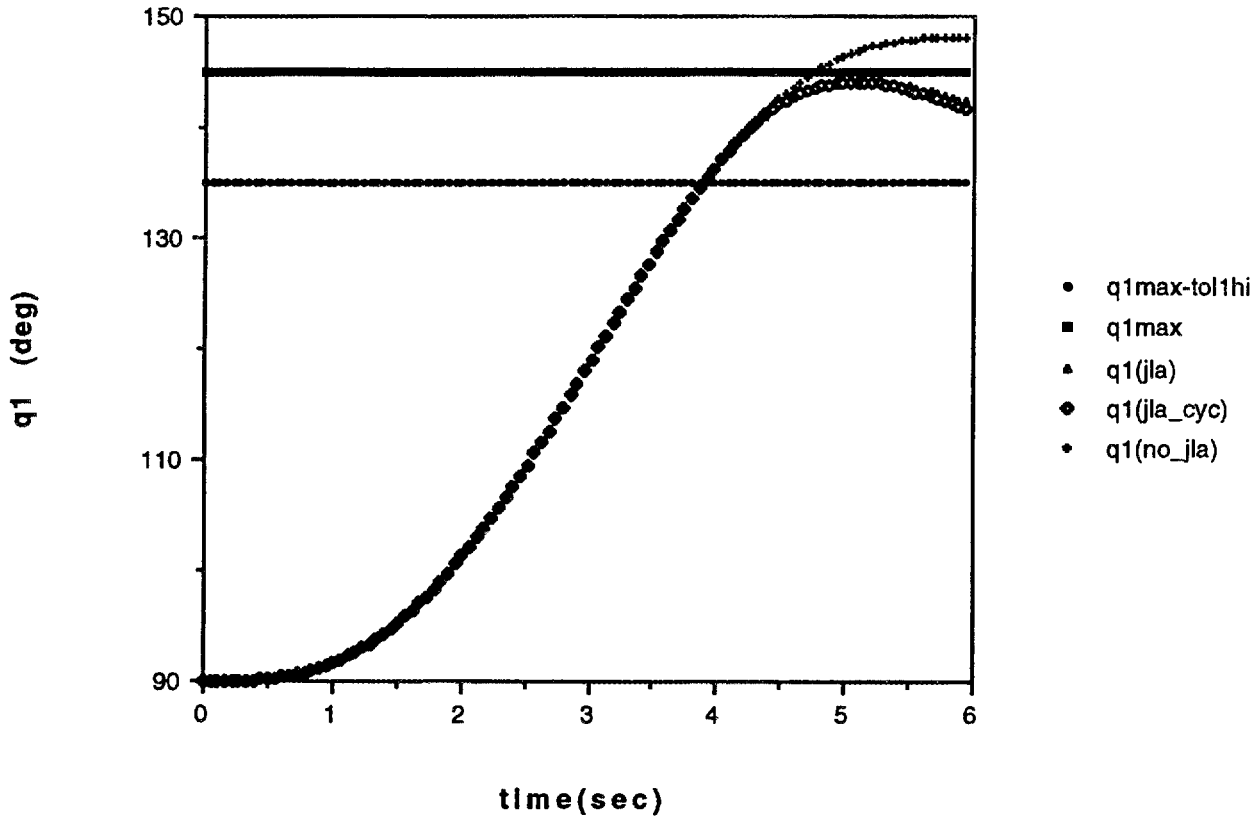


Figure 3.J1A Trajectories for Joint One (Entire Range of Motion)

### CASE 3

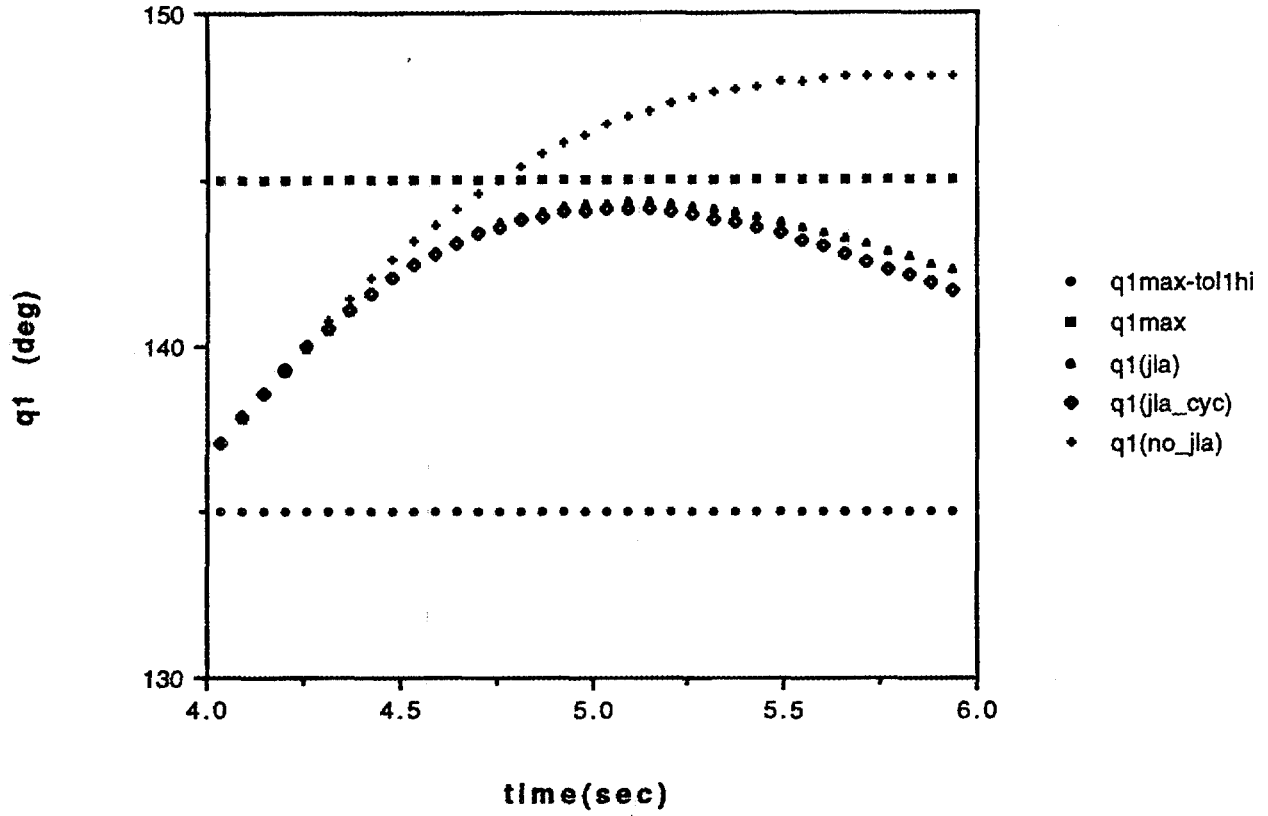


Figure 3.J1B Trajectories for Joint One (Range Where JLA is Active)

### CASE 3

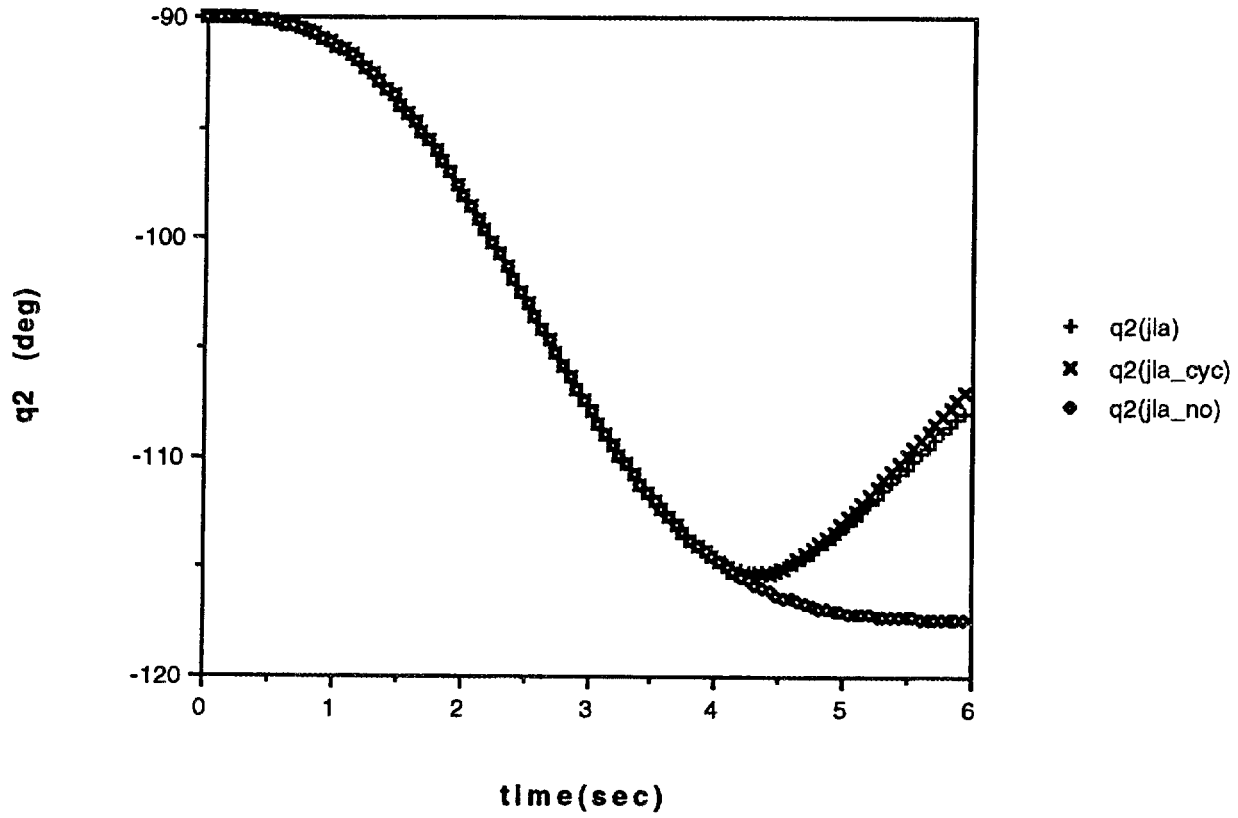


Figure 3.J2A Trajectories for Joint Two (Entire Range of Motion)

### CASE 3

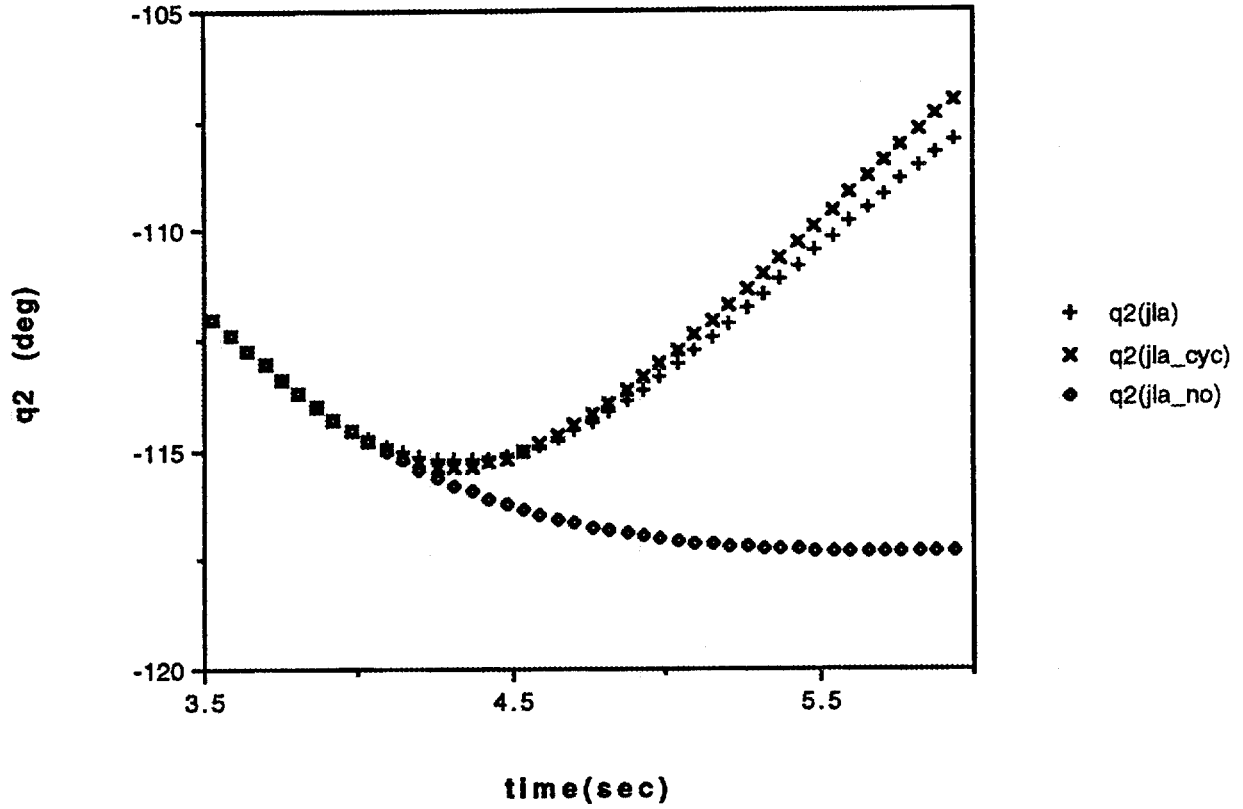


Figure 3.J2B Trajectories for Joint Two (Range Where JLA is Active)

### CASE 3

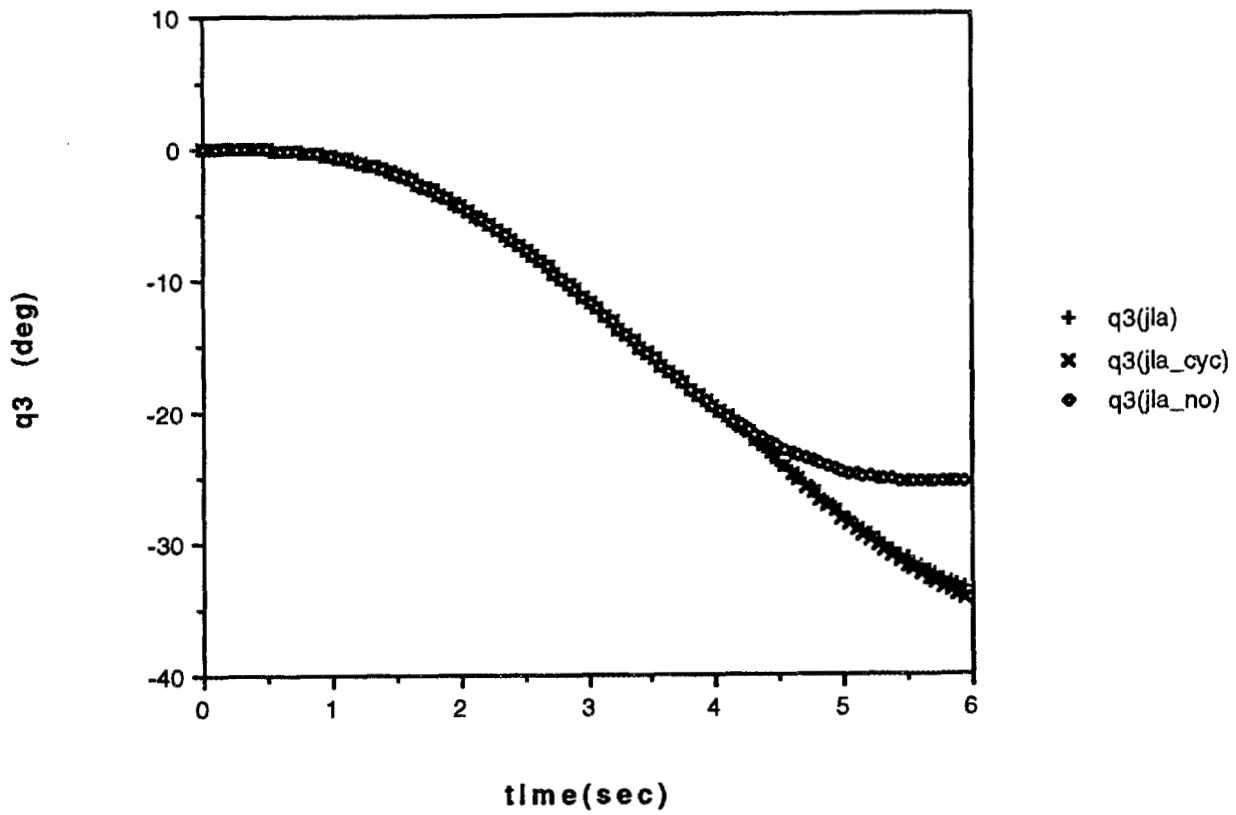


Figure 3.J3A Trajectories for Joint Three (Entire Range of Motion)

### CASE 3

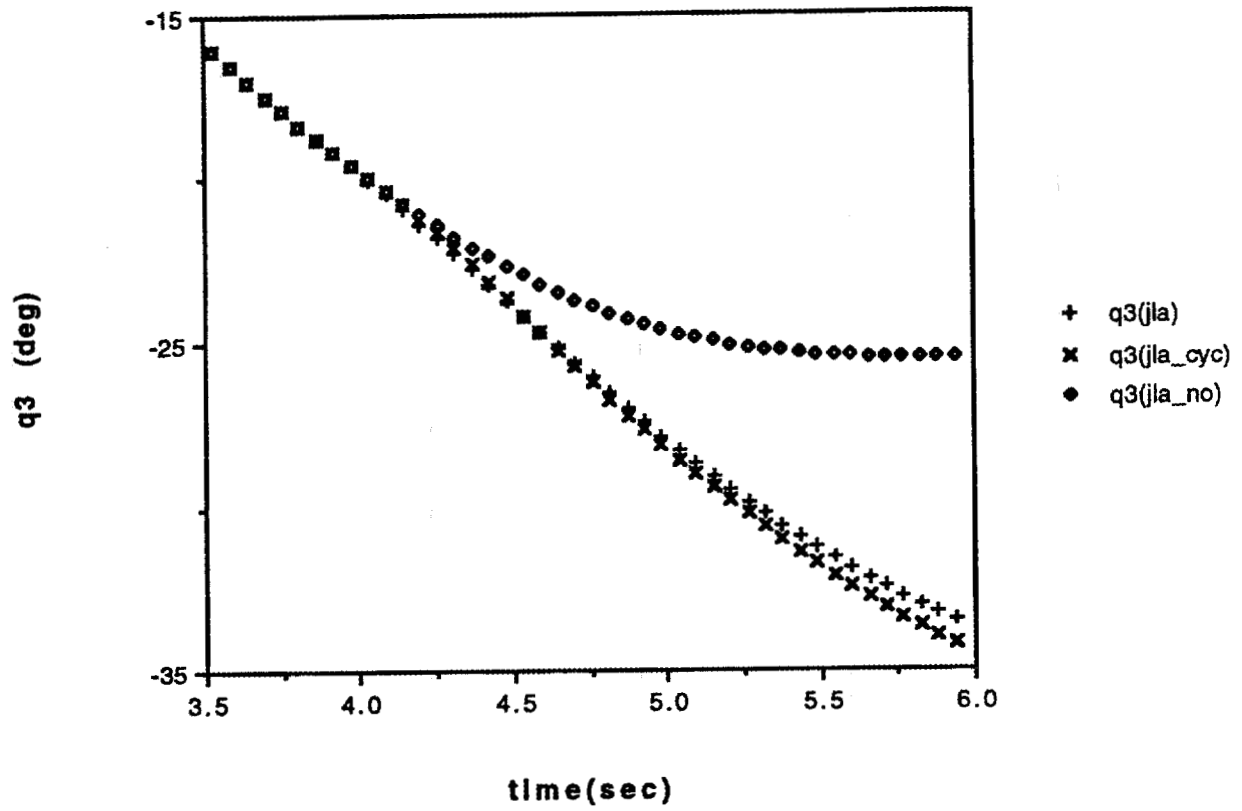


Figure 3.J3B Trajectories for Joint Three (Range Where JLA is Active)

### CASE 3

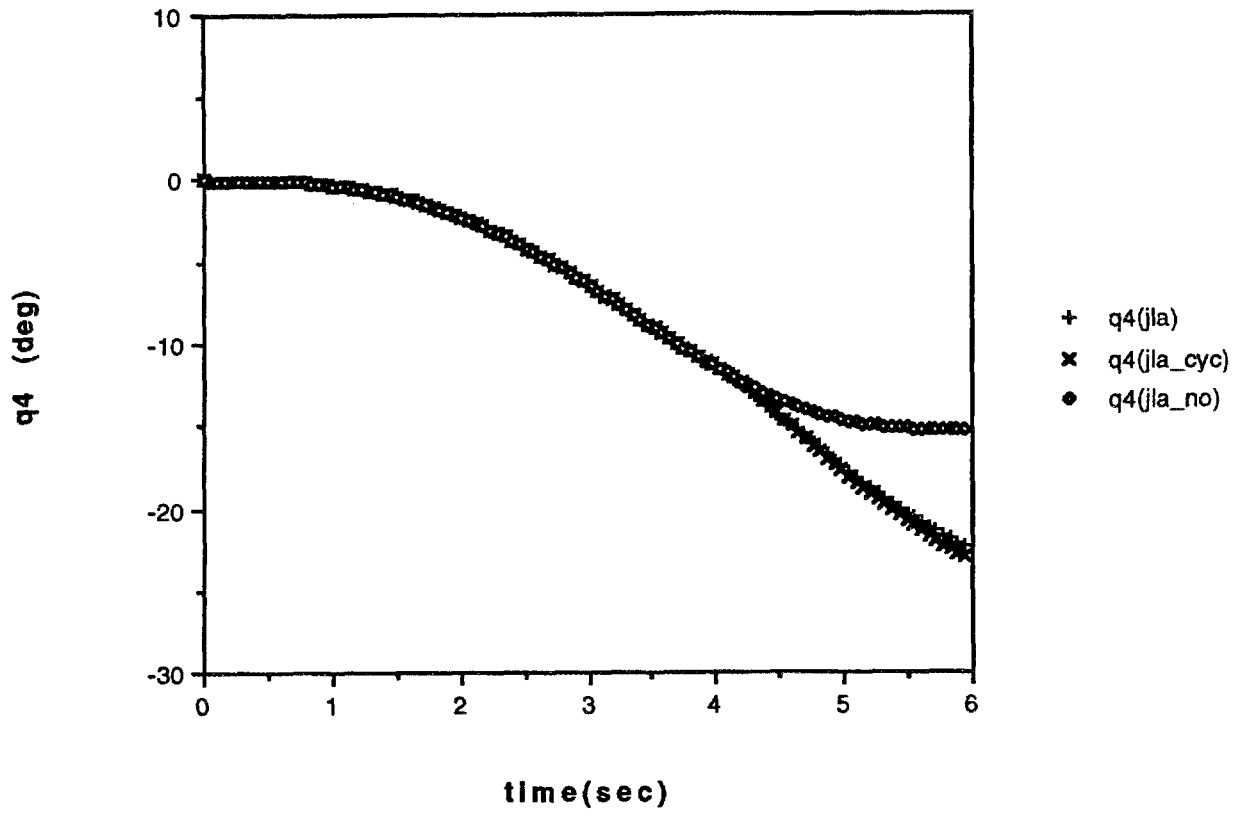


Figure 3.J4A Trajectories for Joint Four (Entire Range of Motion)

### CASE 3

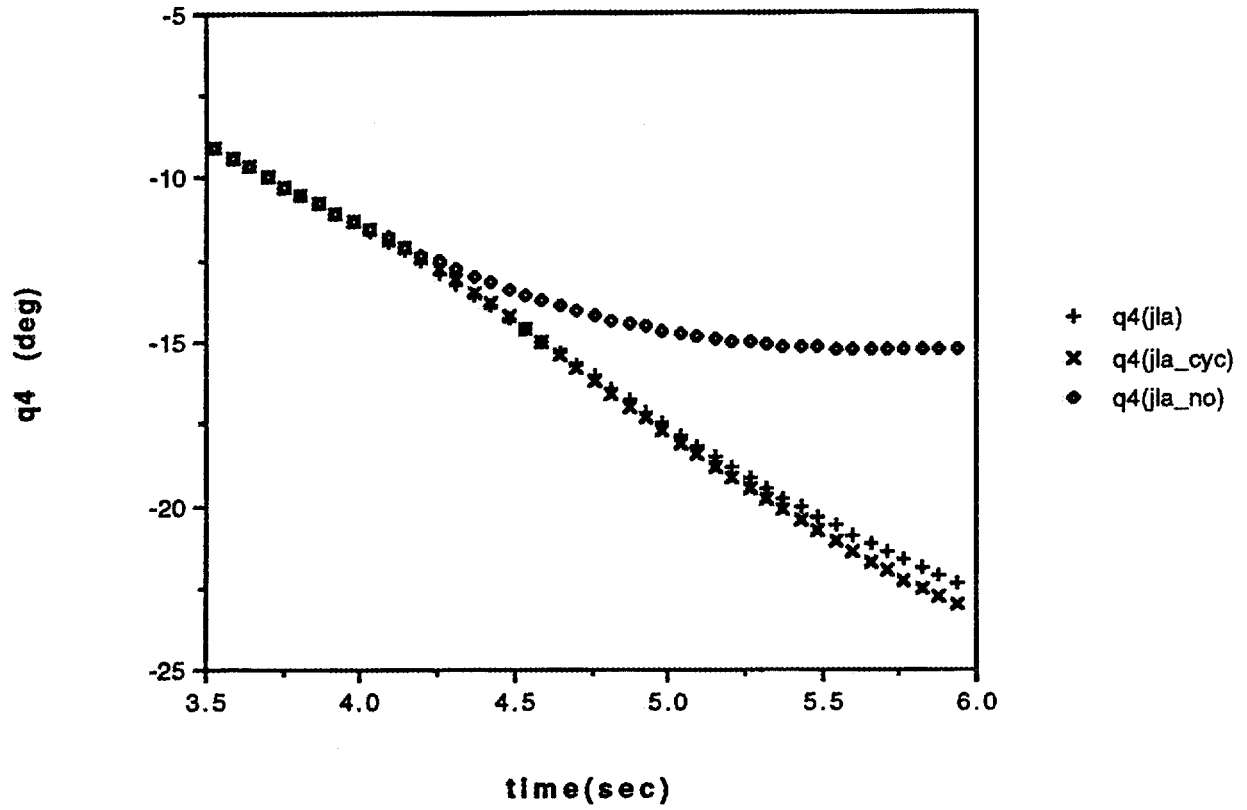


Figure 3.J4B Trajectories for Joint Four (Range Where JLA is Active)

**FIGURES**  
**FOR**  
**CASE FOUR**

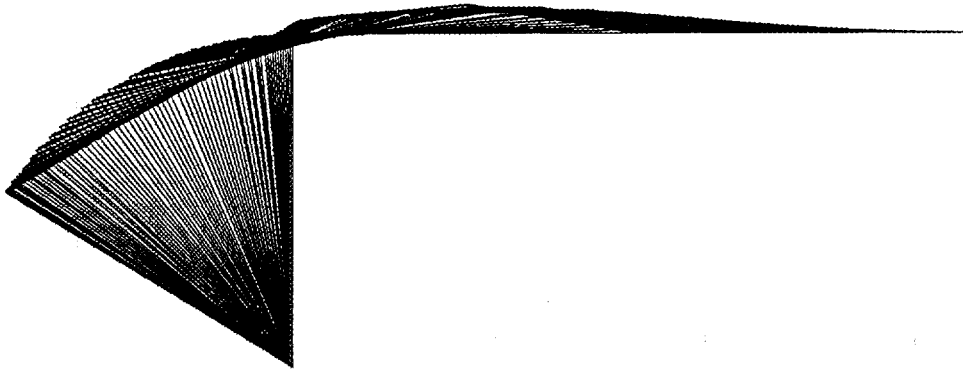


Figure 4.F1 Fan Plot With No JLA (Case 4)

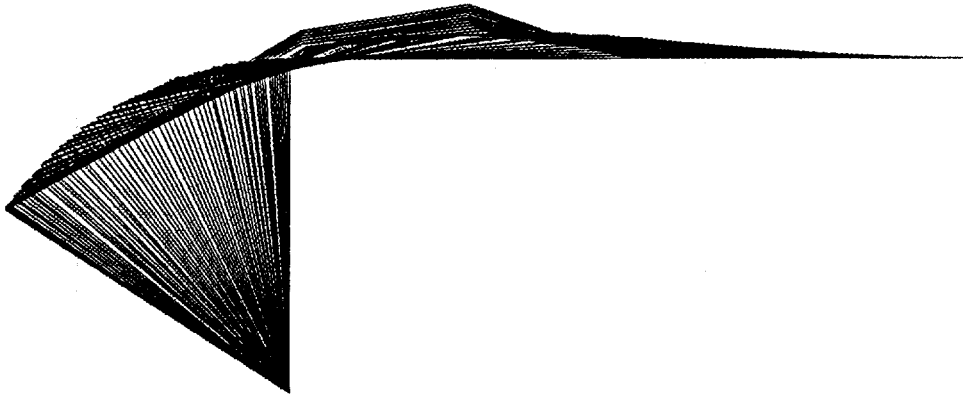


Figure 4.F2 Fan Plot Using Linear JLA Method

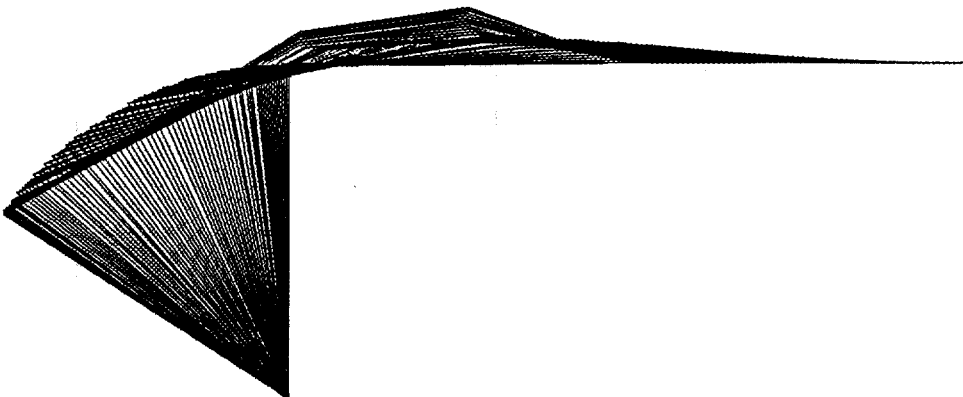


Figure 4.F3 Fan Plot Using Cycloidal JLA Method

### CASE 4

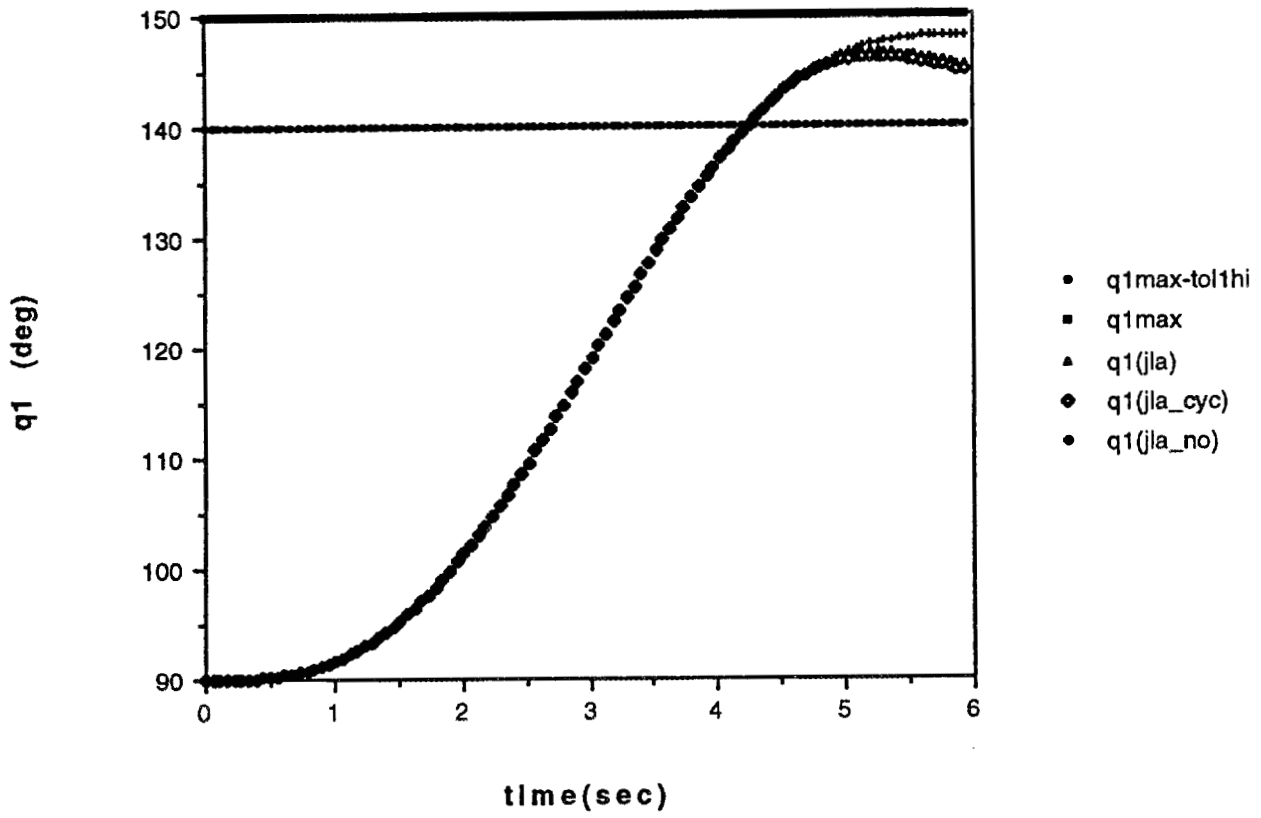


Figure 4.J1A Trajectories for Joint One (Entire Range of Motion)

### CASE 4

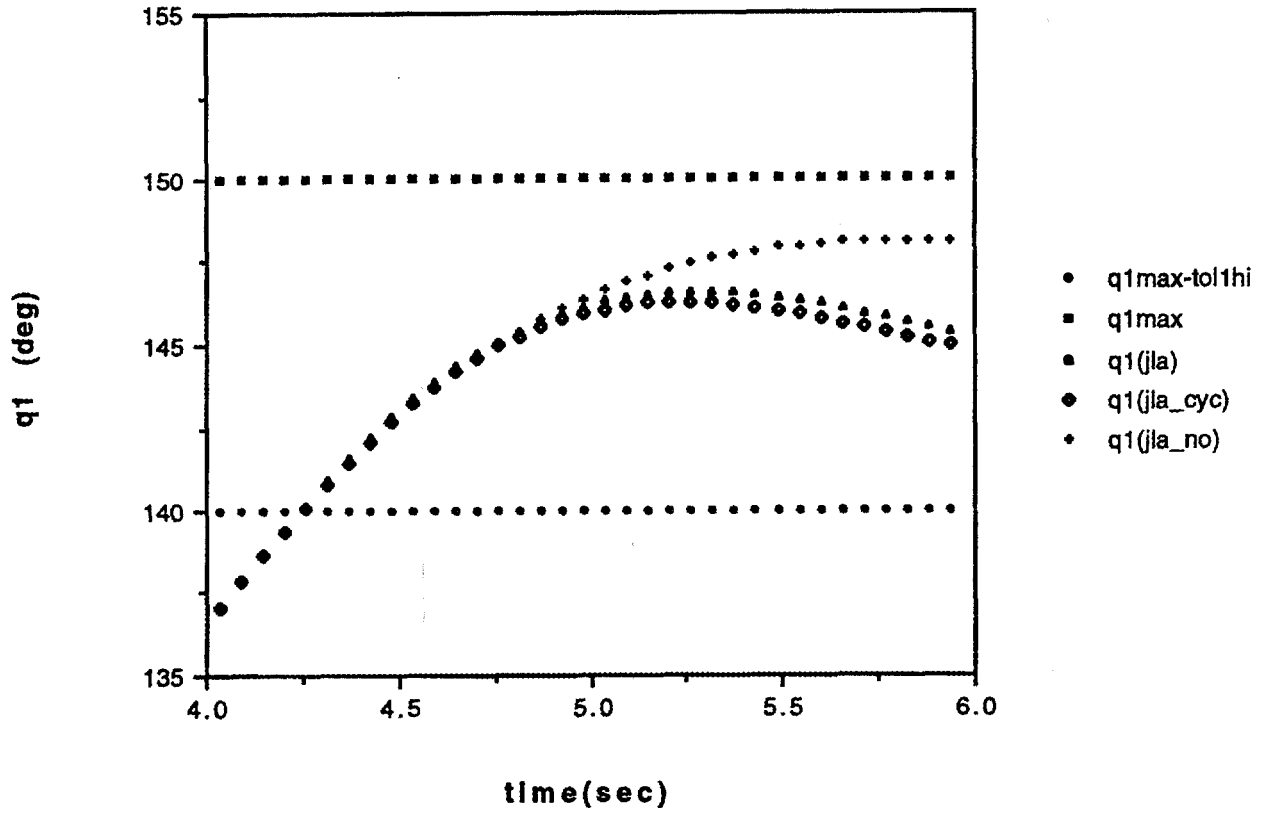


Figure 4.J1B Trajectories for Joint One (Range Where JLA is Active)

### CASE 4

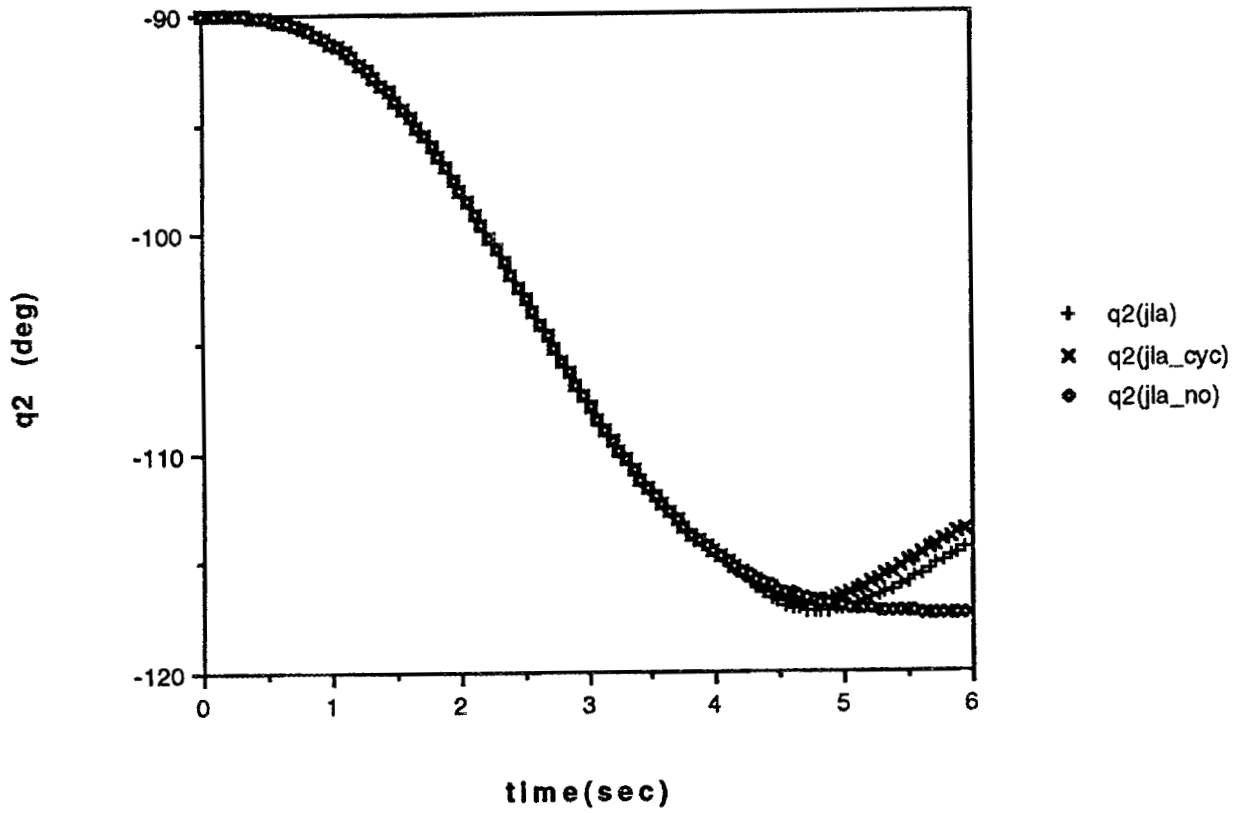


Figure 4.J2A Trajectories for Joint Two (Entire Range of Motion)

### CASE 4

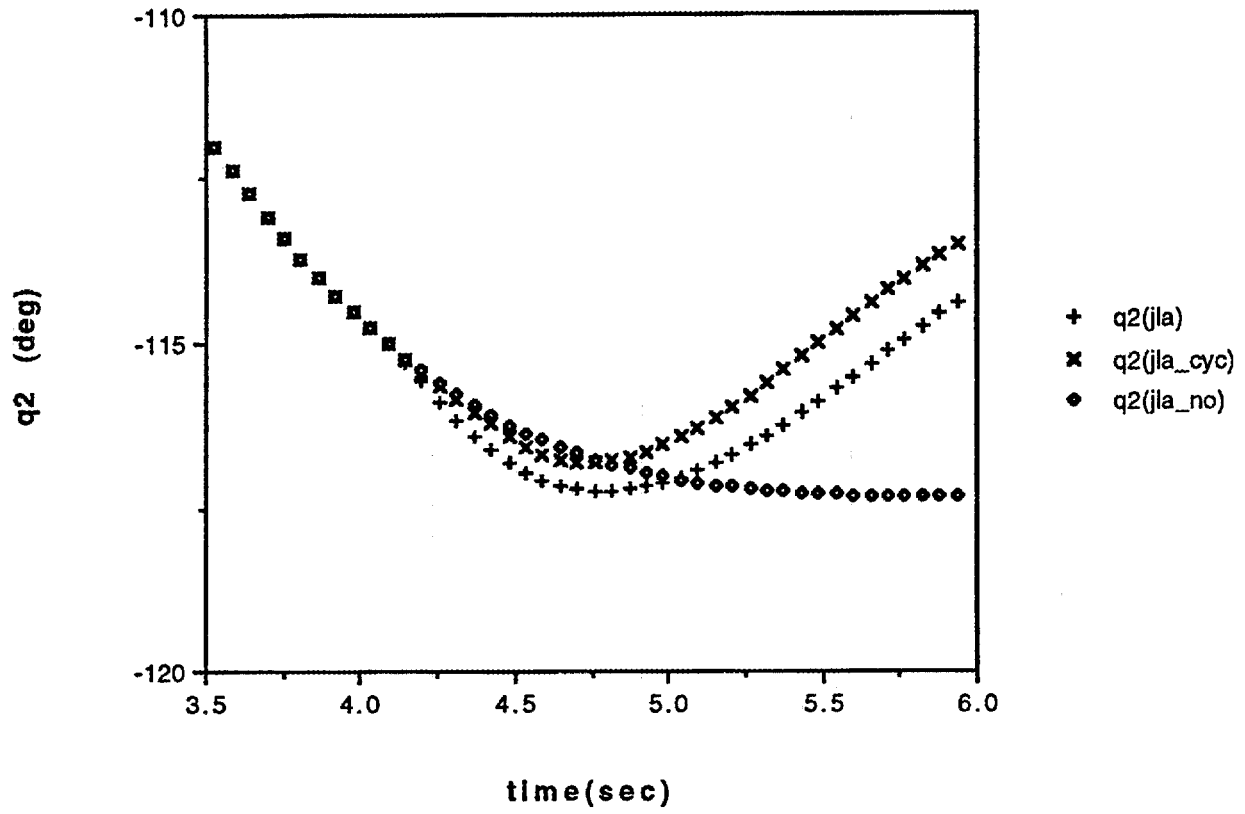


Figure 4.J2B Trajectories for Joint Two (Range Where JLA is Active)

### CASE 4

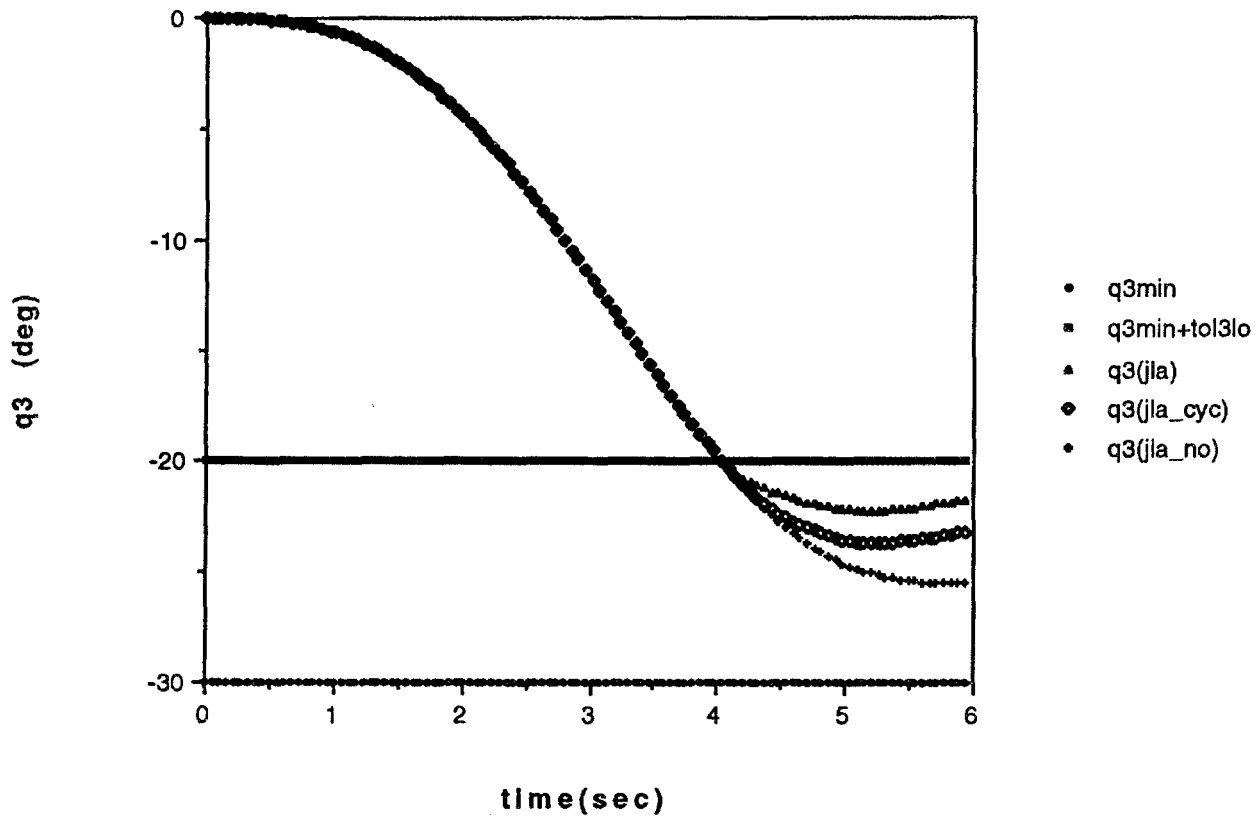


Figure 4.J3A Trajectories for Joint Three (Entire Range of Motion)

### CASE 4

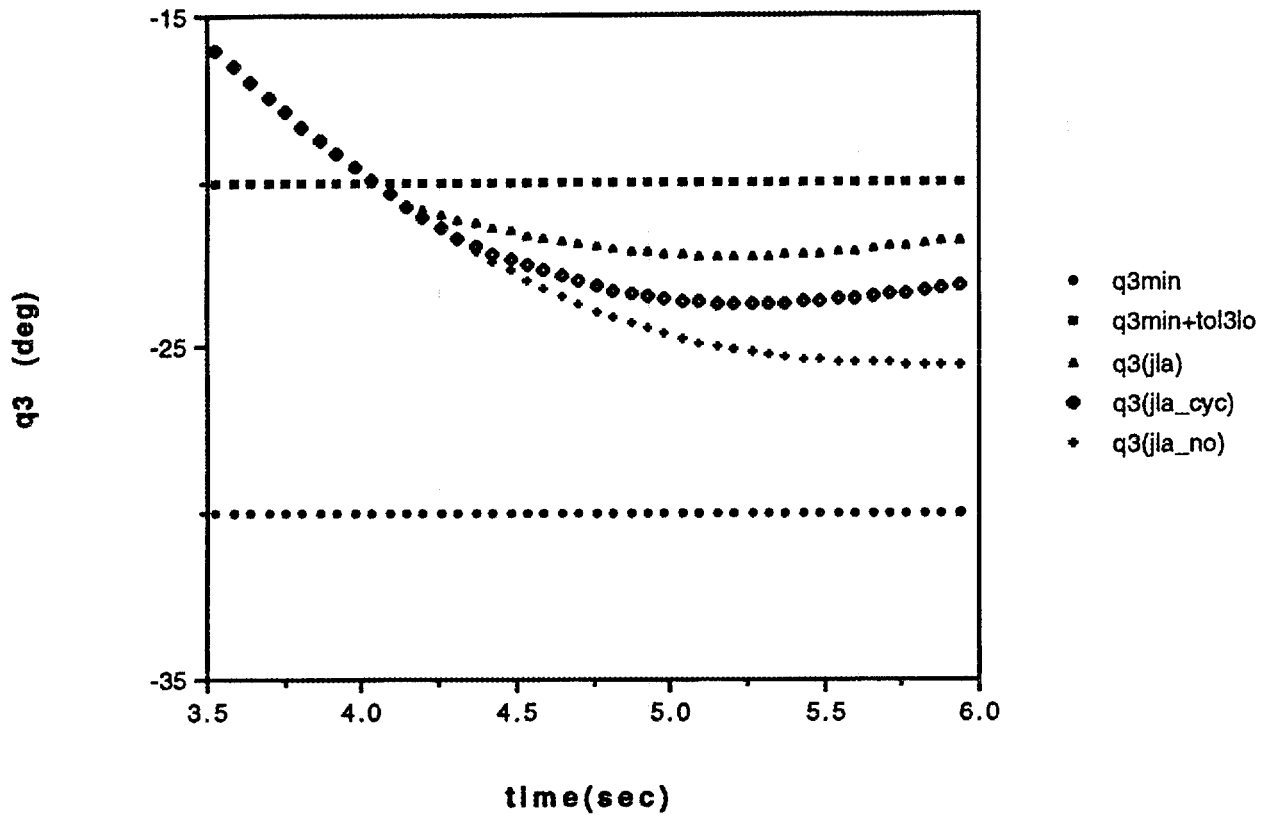


Figure 4.J3B Trajectories for Joint Three (Range Where JLA is Active)

### CASE 4

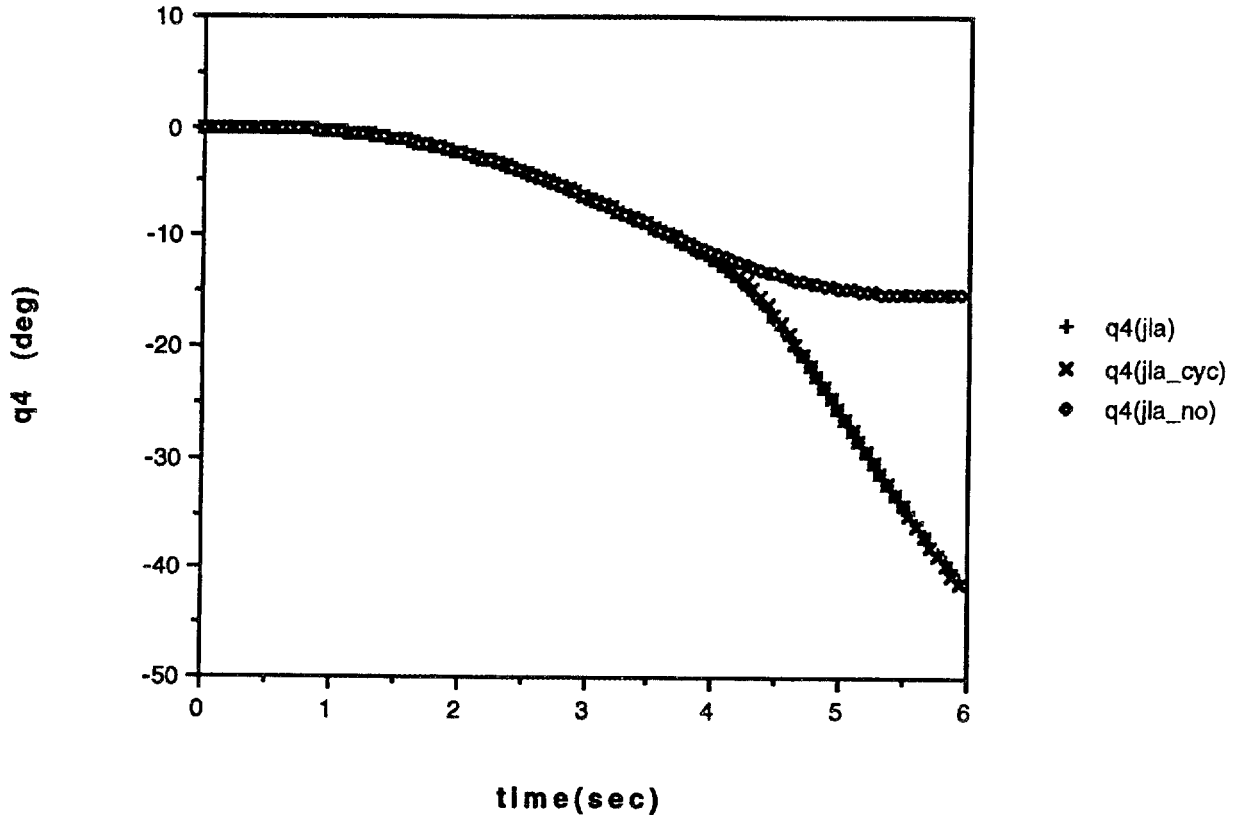


Figure 4.J4A Trajectories for Joint Four (Entire Range of Motion)

### CASE 4

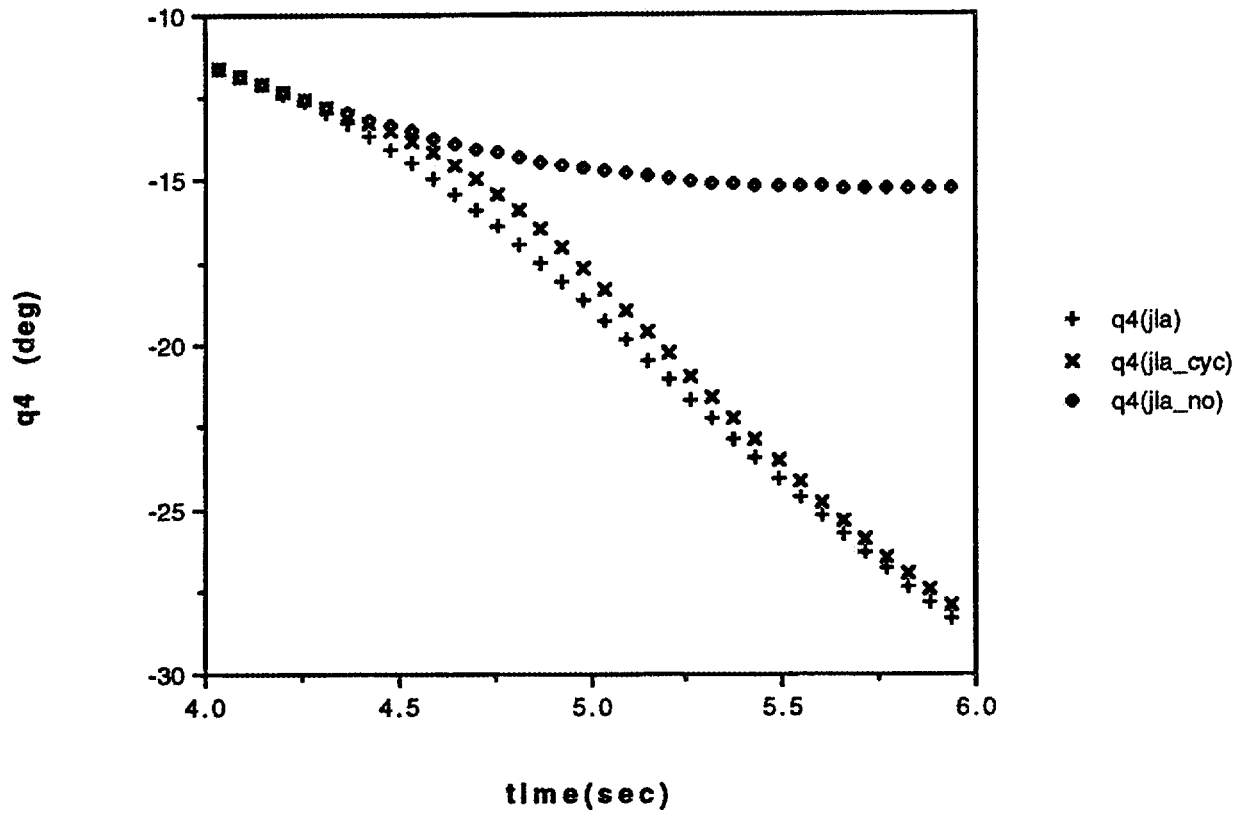
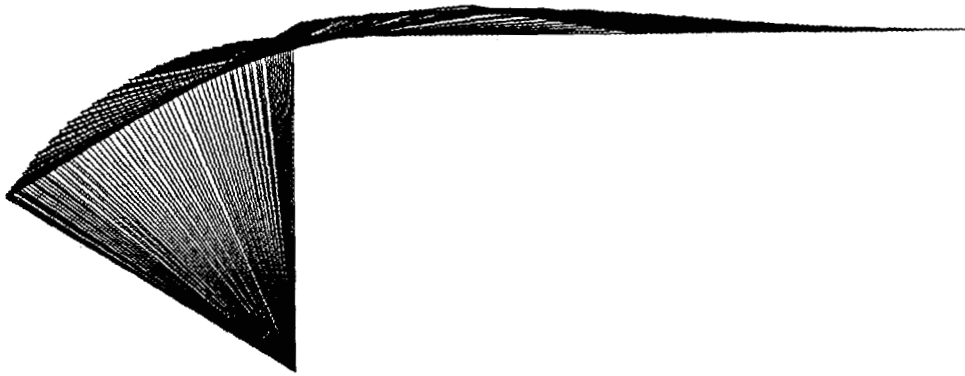
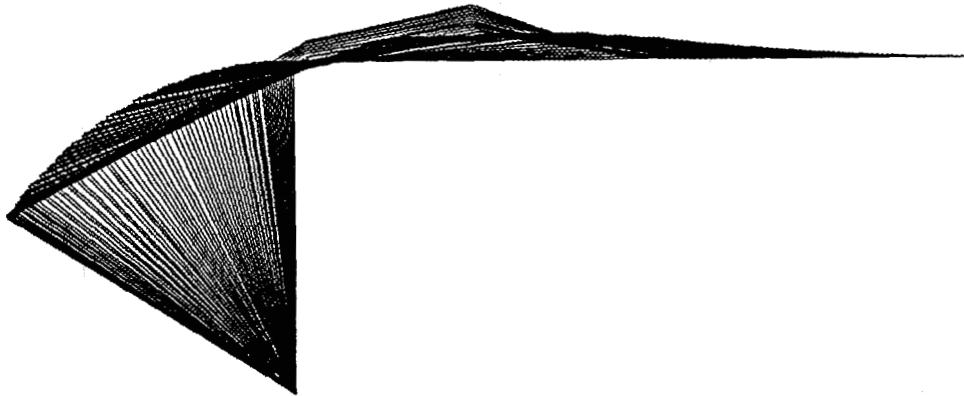


Figure 4.J4B Trajectories for Joint Four (Range Where JLA is Active)

**FIGURES**  
**FOR**  
**CASE FIVE**



**Figure 5.F1 Fan Plot With No JLA (Case 5)**



**Figure 5.F2 Fan Plot Using Linear JLA Method**

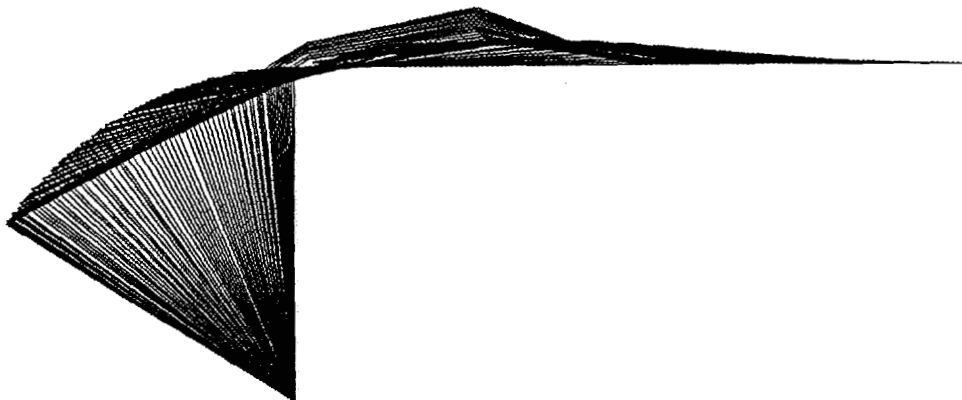


**Figure 5.F3 Fan Plot Using Cycloidal JLA Method**

### CASE 5

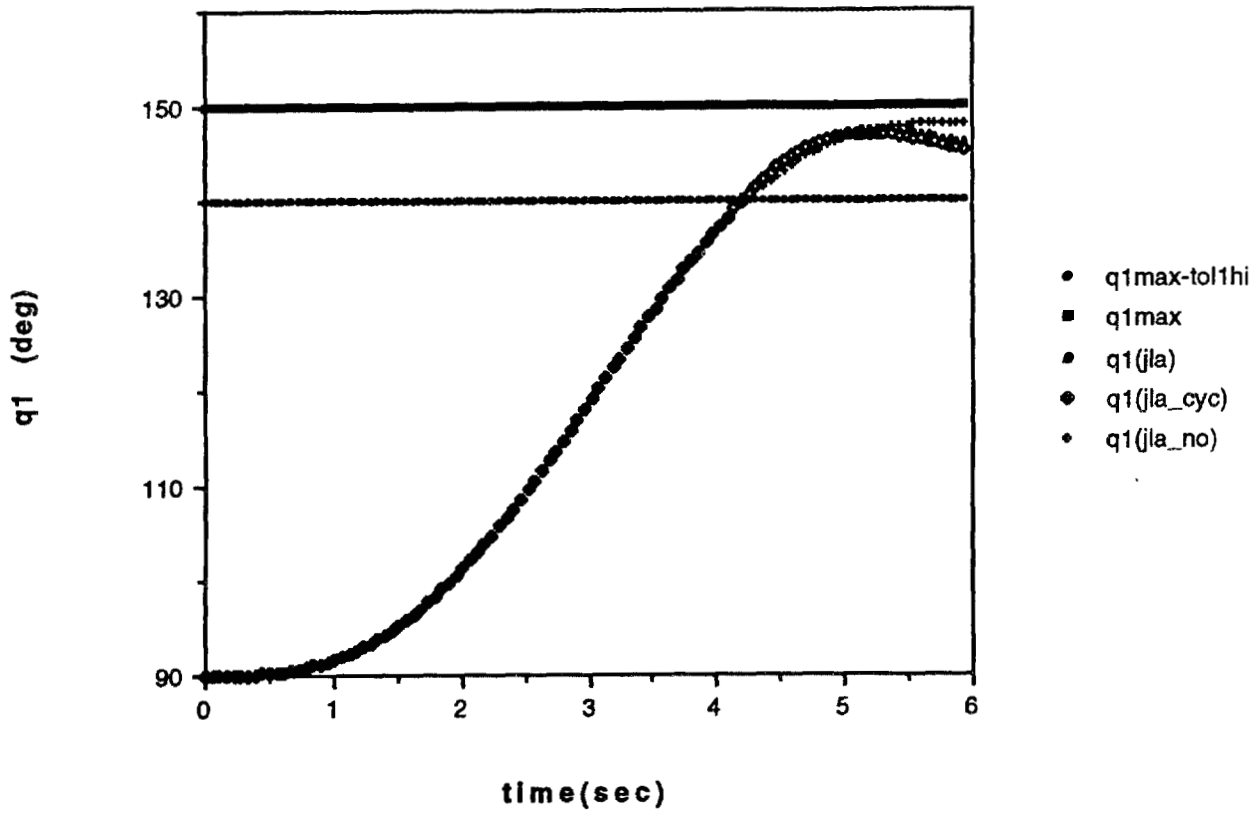


Figure 5.J1A Trajectories for Joint One (Entire Range of Motion)

### CASE 5

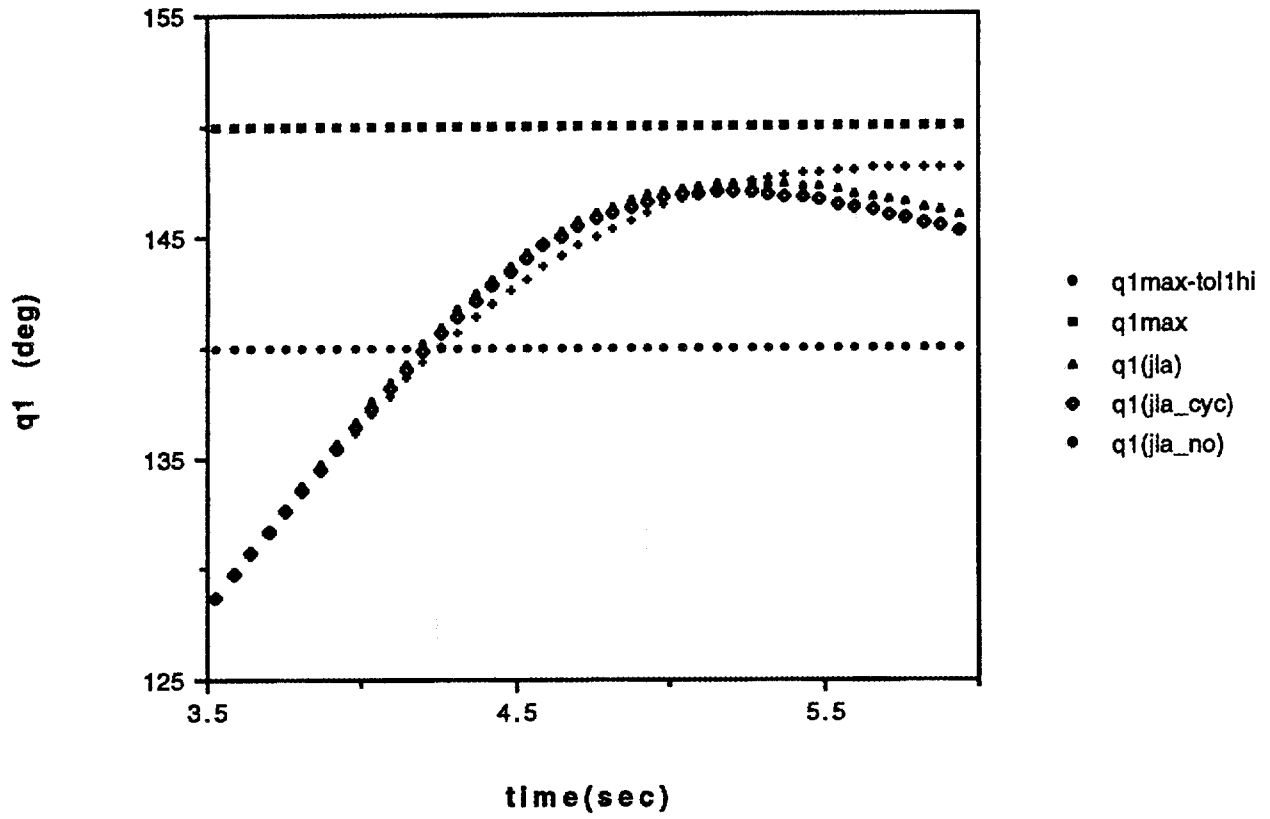


Figure 5.J1B Trajectories for Joint One (Range Where JLA is Active)

### CASE 5

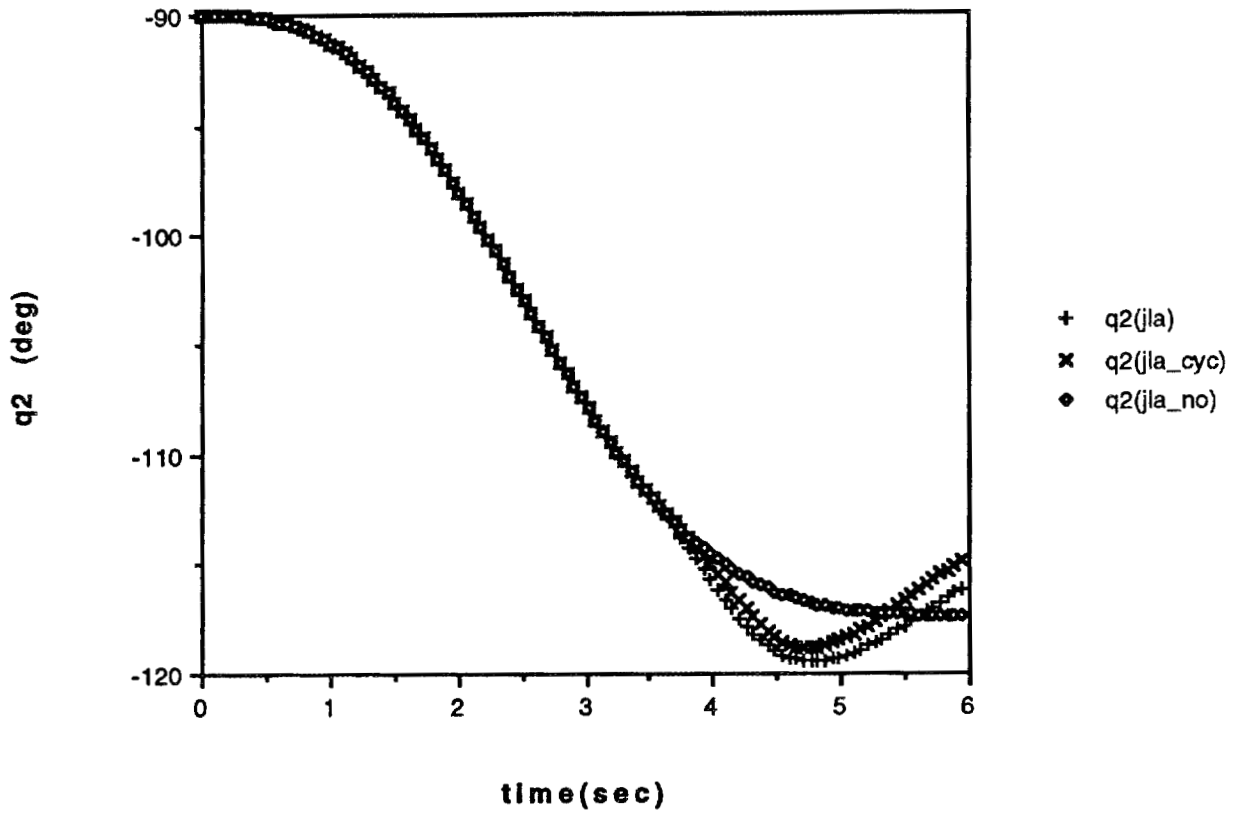


Figure 5.J2A Trajectories for Joint Two (Entire Range of Motion)

### CASE 5

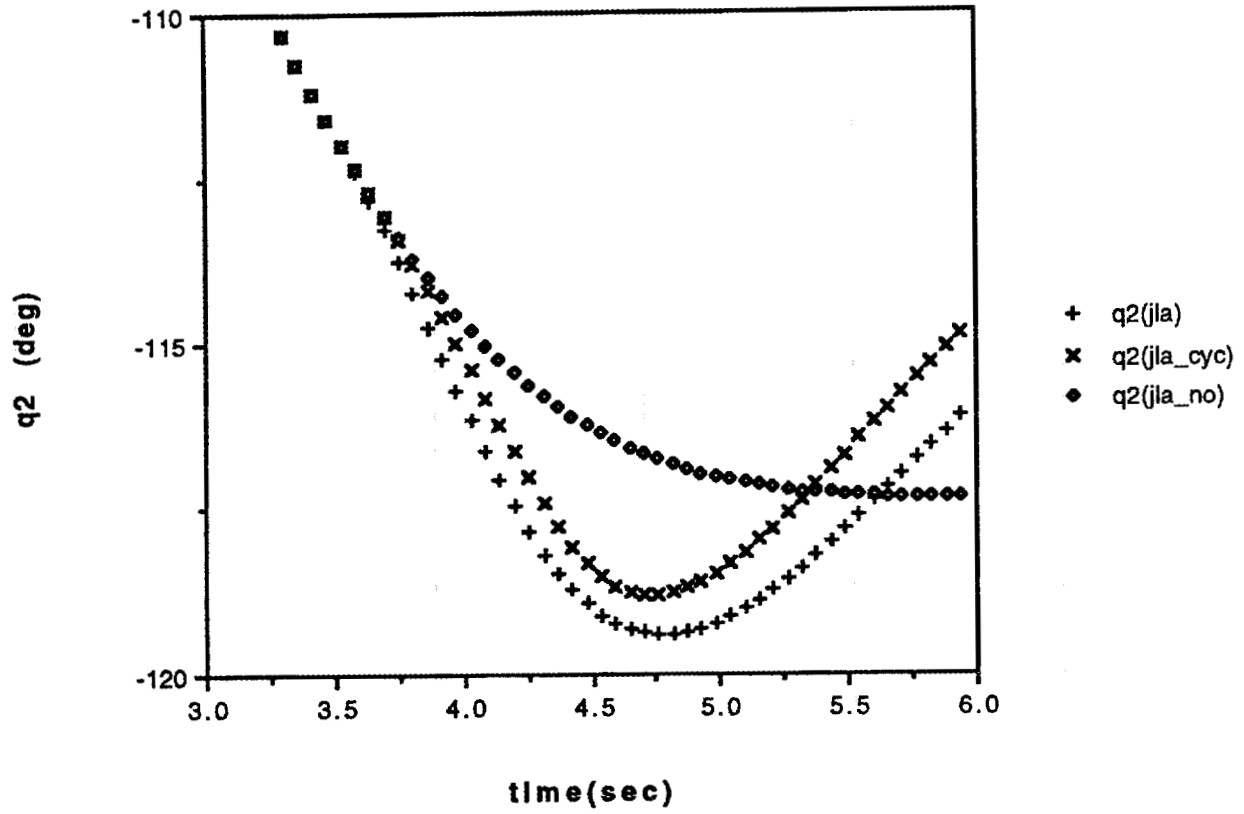


Figure 5.J2B Trajectories for Joint Two (Range Where JLA is Active)

### CASE 5

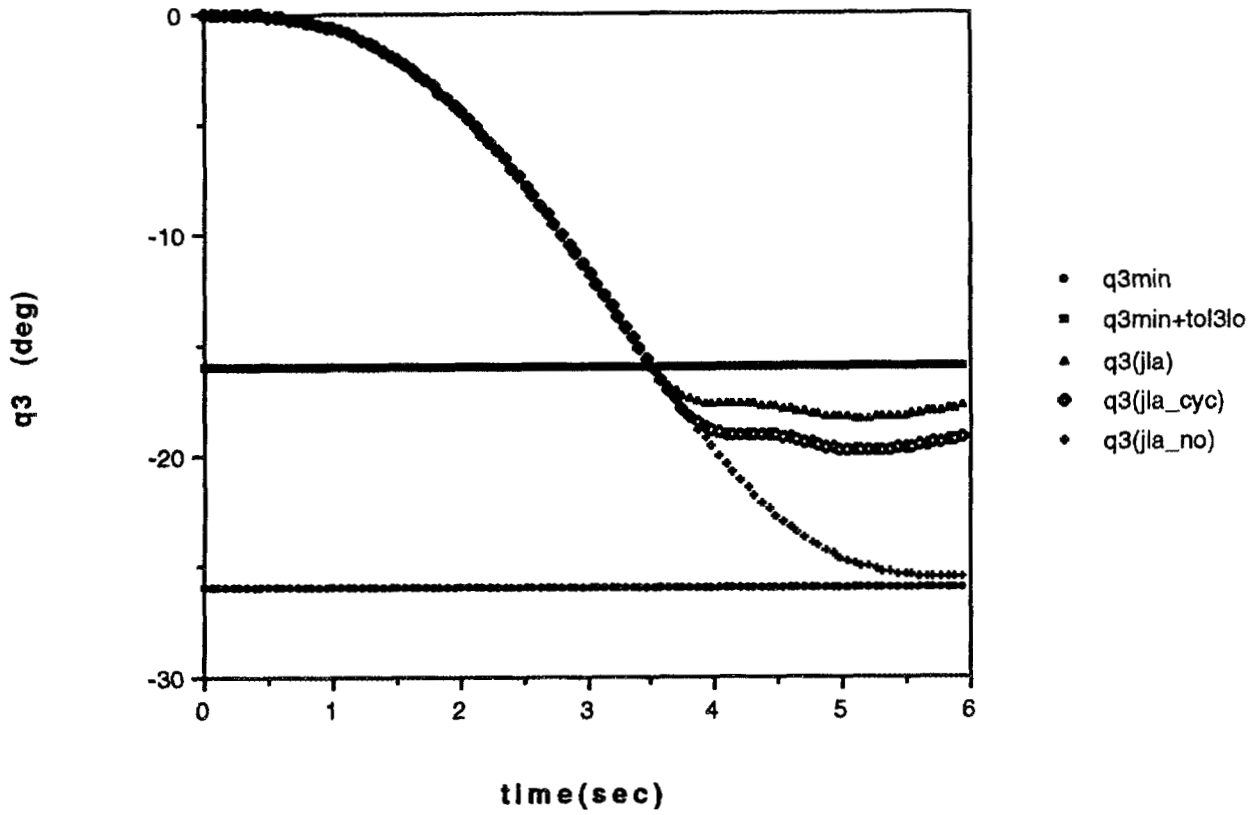


Figure 5.J3A Trajectories for Joint Three (Entire Range of Motion)

### CASE 5

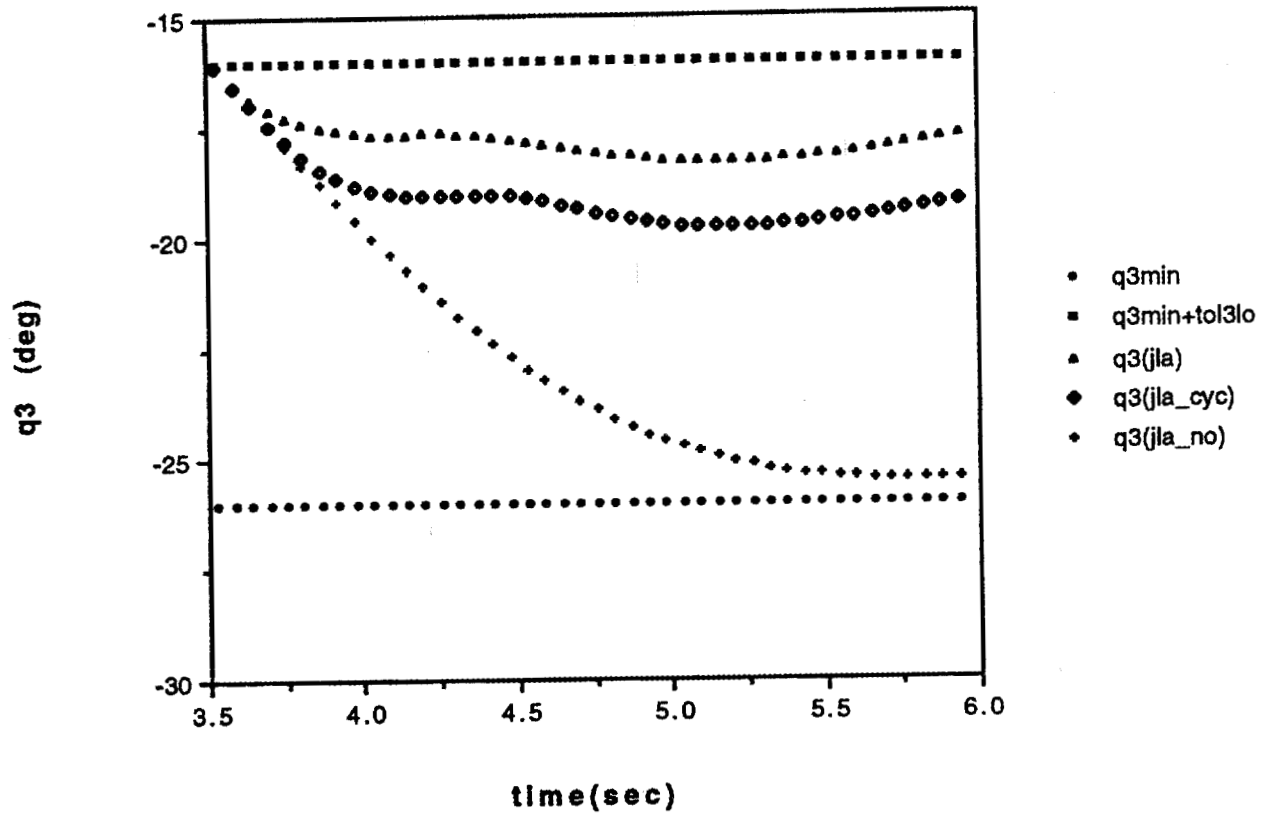


Figure 5.J3B Trajectories for Joint Three (Range Where JLA is Active)

### CASE 5

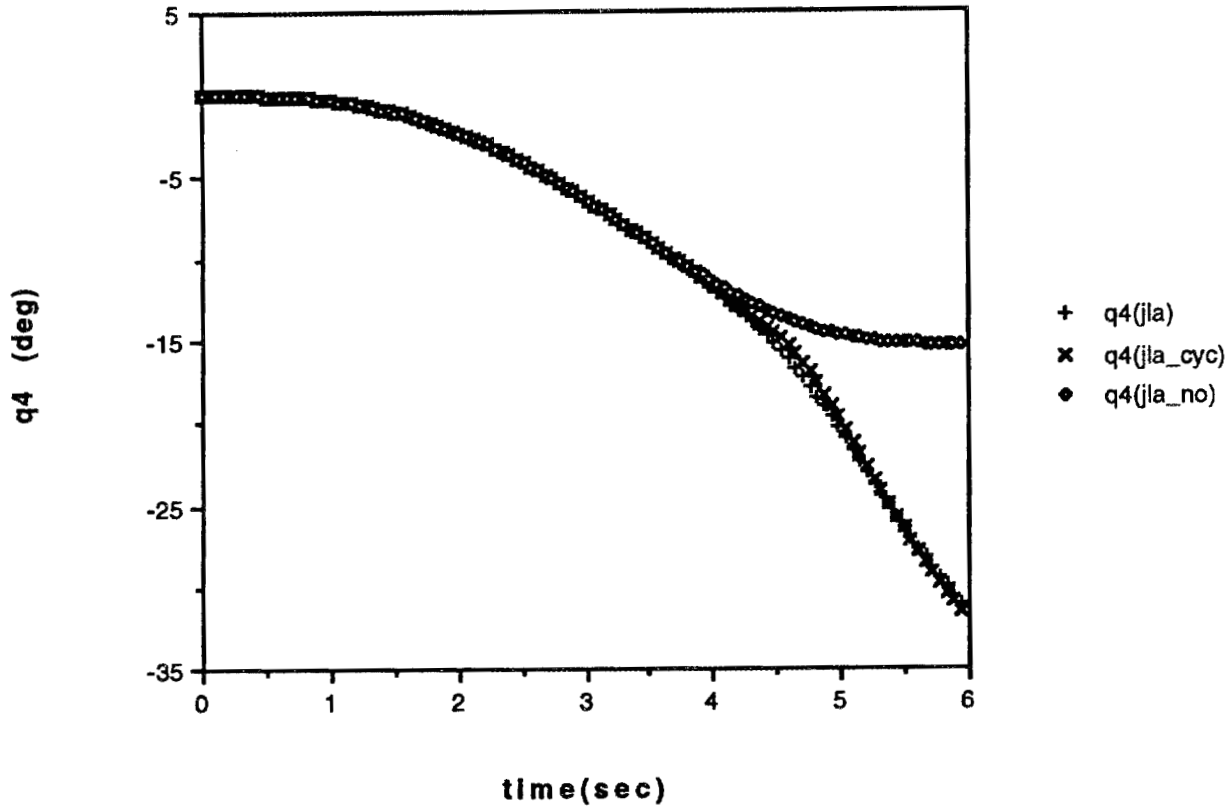


Figure 5.J4A Trajectories for Joint Four (Entire Range of Motion)

CASE 5

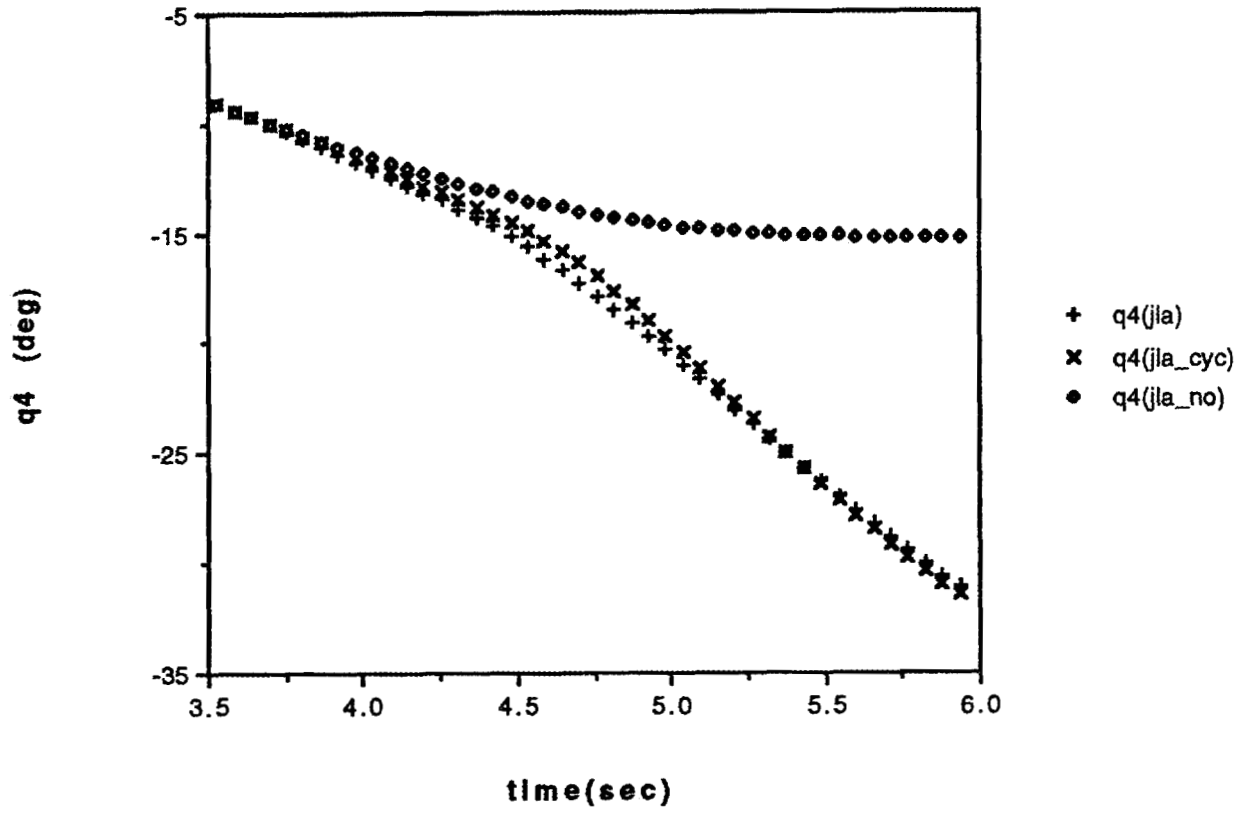


Figure 5.J4B Trajectories for Joint Four (Range Where JLA is Active)



## 5 Conclusion

A new approach has been suggested for the avoidance of joint limits during motion of a redundant manipulator. The entire range of motion for each joint has been divided into three subranges. When a joint lies in either outer subrange, it is considered to be in close proximity to a hardware limit and it is desired to move the joint back into the inner (center) region via self motion of all joints. This can be accomplished through an application of the general secondary performance criteria and inverse kinematics procedure described in Part 2 of this report [6]. The problem studied in Part 3 has been how to calculate the corrective joint velocity vector  $\dot{q}^*$  that is an explicit variable in the symbolic solution for the joint velocities so as to accomplish the joint limit avoidance. Two methods have been suggested for calculating  $\dot{q}^*$ . In both methods, the components of  $\dot{q}^*$  corresponding to those joints lying in their outer regions are calculated such that their magnitudes are a function of how close they are to their limits and their signs are selected so as to move the joints away from the respective limits. The components of  $\dot{q}^*$  corresponding to the joints lying in their center ranges are set to zero.

The  $i$ th component of  $\dot{q}^*$  is defined as a linear function of  $q_i$  in the upper and lower prohibitive subranges of motion using the first method. However, it was found that  $\dot{q}_i^*$  is not pointwise differentiable at the transition points between the three subranges of motion. To overcome this deficiency, it was proposed to define  $\dot{q}_i^*$  by cycloidal functions when  $q_i$  lies in either outer range. The resulting function is sectionally smooth, uniformly continuous, and pointwise differentiable throughout the entire range of motion of joint  $i$ .

Both algorithms were devised such that if none of the joints lie in their outer regions, no corrective action is taken. In this case the term explicit in  $\dot{q}^*$  in the symbolic solution for the joint velocities derived in Part 2 vanishes which reduces the computations and yields a minimum norm solution for the joint velocities.

The algorithms were tested through simulating a planar manipulator with four revolute joints with two degrees of redundancy. The performance of the algorithms was tested in the cases where only one or multiple joints simultaneously moved in their respective prohibitive ranges of motion.



## **6 Acknowledgement**

This research was sponsored by the Office of Engineering Research Program, Basic Energy Sciences, of the U.S. Department of Energy, under contract DE-AC05-84OR21400 with Lockheed Martin Energy Systems, Inc.



## References

- [1] D.N. Nenchev, "Redundancy Resolution through Local Optimization: A Review," *J. of Robotic Systems* Vol. 6, No. 6, pp. 769-798, December 1989.
- [2] B. Siciliano, "Kinematic Control of Redundant Robot Manipulators: A Tutorial," *J. of Intelligent and Robotic Systems* Vol. 3, pp. 201-212, 1990.
- [3] A. Liegeois, "Automatic Supervisory Control of the Configuration and Behavior of Multibody Mechanisms," *IEEE Trans. Systems, Man, and Cybernetics*, vol. smc-7, no. 12, 1977, pp. 868-871.
- [4] C.A. Klein and C-H. Huang, "Review of Pseudoinverse Control for Use with Kinematically Redundant Manipulators," *IEEE Trans. Systems, Man, and Cybernetics*, vol. smc-13, no. 3, March/April 1983, pp. 245-250.
- [5] C.A. Klein and A.I. Chirco, "Dynamic Simulation of a Kinematically Redundant Manipulator System," *J. Robotic Systems*, vol. 4, no. 1, Feb. 1987, pp. 5-23.
- [6] M.A. Unseren, "New Insights Into Input Relegation Control for Inverse Kinematics of a Redundant Manipulator. Part 2: The Optimization of a Secondary Criteria Involving Self Motion of the Joints," Oak Ridge National Laboratory Technical Report No. ORNL/TM-12813 (Part 2), June 1995.
- [7] F.G. Pin, M. Beckerman, P.F. Spelt, J.T. Robinson, and C.R. Weisbin, "Autonomous Mobile Robot Research Using the Hermies-III Robot," *IEEE/RSJ Int'l Workshop on Intelligent Robots and Systems '89*, September 4-6, 1989, Tsukuba, Japan, pp. 251-256.
- [8] C.R. Weisbin, B.L. Burks, J.R. Einstein, R.R. Feezell, W.W. Manges, and D.H. Thompson, "HERMIES-III: A Step Toward Autonomous Mobility, Manipulation and Perception," *Robotica*, Vol. 8, Part 1, January-March 1990, pp 7-12.
- [9] J.N. Anderson and W.D. Combs, "Link Mass Properties of the CESAR Research Manipulator," Martin Marietta Energy Systems, Inc. Technical Report No. MCTR-0987-14, September 1987.
- [10] V.M. Faires, *Kinematics*, McGraw-Hill Book Co., 1959.
- [11] H. Seraji, "Adaptive Independent Joint Control of Manipulators: Theory and Experiment," *Proc. IEEE Int'l Conf. on Robotics and Automation*, Vol. 2, pp. 854-861, Philadelphia PA, April 24-29, 1988.

## INTERNAL DISTRIBUTION

- |                      |                                      |
|----------------------|--------------------------------------|
| 1-5. J. Barhen       | 31. F. G. Pin                        |
| 6. M. Beckerman      | 32. N. S. V. Rao                     |
| 7. C. W. Glover      | 33-37. D. B. Reister                 |
| 8-12. W. C. Grimmell | 38. S. Shekhar                       |
| 13. J. F. Jansen     | 39-43. R. F. Sincovec                |
| 14. J. P. Jones      | 44. D. Thompson                      |
| 15. H. E. Knee       | 45. E. C. Uberbacher                 |
| 16. R. L. Kress      | 46-50. M. A. Unseren                 |
| 17. D. S. Kwon       | 51. CSMD Reports Office              |
| 18-22. R. C. Mann    | 52-53. Laboratory Records Department |
| 23. M. D. Morris     | 54. Laboratory Records, ORNL-RC      |
| 24. E. M. Oblow      | 55. Document Reference Section       |
| 25-29. C. E. Oliver  | 56. Central Research Library         |
| 30. L. E. Parker     | 57. ORNL Patent Office               |

## EXTERNAL DISTRIBUTION

58. Dr. Fred Aminzadeh, 401 Paseo Estrella, Anaheim Hills, CA 92807
59. Dr. John S. Bay, Bradley Department of Electrical Engineering, Virginia Polytechnic Institute and State University, Blacksburg, VA 24061
60. Dr. John Blair, JBX Technologies, 25 Moore Road, Wayland, MA 01778
61. Professor Roger W. Brockett, Harvard University, Pierce Hall, 29 Oxford St., Cambridge, MA 02138
62. Dr. H. Hemami, Ohio State University, Department of Electrical Engineering, Columbus, Ohio 43210
63. Mr. Steve Holland, Robotics, B/MD-63, General Motors Corporation, NAO Manufacturing Center, 30300 Mound Rd., Warren, MI 48090-9040
64. Professor Takeo Kanade, Computer Science and Robotics, Carnegie Mellon University, Pittsburgh, PA 15213-3890

65. Dr. Oscar P. Manley, Division of Engineering, Mathematical, and Geosciences, Office of Basic Energy Sciences, ER-15, U.S. Department of Energy, Germantown, Washington, DC 20545
66. Dr. K. S. Narendra, Yale University, Center for Systems Science, Department of Electrical Engineering, P.O. Box 208267, New Haven, CT 06520-8267
67. R. D. Rafler, 8906 Talbot Avenue, Silver Spring, MD 20910
68. Dr. Rodney Roberts, FAMU/FSU, College of Engineering, Department of Electrical Engineering, 2525 Pottsdamer Street, Tallahassee, FL 32310
69. Dr. Wes Snyder, Department of Radiology, Bowman Gray School of Medicine, N.C. Baptist Hospital School of Medicine, 300 S. Hawthorne Dr., Winston-Salem, NC 27103
70. Professor Mary F. Wheeler, Department of Mathematical Sciences, Rice University, P.O. Box 1892, Houston, TX 77251
71. Dr. Yong Zhou, 14616 NE 36th, Apt #E-13, Bellevue, WA 98007
72. Office of Assistant Manager for Energy Research and Development, U.S. Department of Energy, Oak Ridge Operations Office, P.O. Box 2001, Oak Ridge, TN 37831-8600
- 73-74. Office of Scientific & Technical Information, P. O. Box 62, Oak Ridge, TN 37830